RADC-TR-82-320
Interim Report
December 1982

ACOSS TWELVE (Active Control of Space Structures)

Lockheed Missiles & Space Company, Inc.

Sponsored by
Defense Advanced Research Projects Agency (DOD)
ARPA Order No. 3654

APPROVED FOR PUBLIC RELEASE; DISTRIBUTION UNLIMITED

The views and conclusions contained in this document are those of the authors and should not be interpreted as necessarily representing the official policies, either expressed or implied, of the Defense Advanced Research Projects Agency or the U.S. Government.

ROME AIR DEVELOPMENT CENTER
Air Force Systems Command
Griffiss Air Force Base, NY 13441

This report has been reviewed by the RADC Public Affairs Office (PA) and is releasable to the National Technical Information Service (NTIS). At NTIS it will be releasable to the general public, including foreign nations.

RADC-TR-82-320 has been reviewed and is approved for publication.

APPROVED: Richard W. Carman

RICHARD W. CARMAN
Project Engineer

APPROVED: Frank J. Rehm

FRANK J. REHM
Technical Director
Surveillance Division

FOR THE COMMANDER: John P. Huss

JOHN P. HUSS
Acting Chief, Plans Office

If your address has changed or if you wish to be removed from the RADC mailing list, or if the addressee is no longer employed by your organization, please notify RADC (OCSE) Griffiss AFB NY 13441. This will assist us in maintaining a current mailing list.

Do not return copies of this report unless contractual obligations or notices on a specific document requires that it be returned.

ACOSS TWELVE (ACTIVE CONTROL OF SPACE STRUCTURES)

Jean N. Auburn

Contractor: Lockheed Missiles and Space Company
Contract Number: F30602-81-C-0260
Effective Date of Contract: 22 July 1981
Contract Expiration Date: 22 September 1982
Short Title of Work: ACOSS TWELVE
Program Code Number: 2E20
Period of Work Covered: Aug 81 - Apr 82

Principal Investigator: Arthur A. Woods
Phone: 408 742-3568

Project Engineer: Richard W. Carman
Phone: 315 330-3148

This research was supported by the Defense Advanced Research Projects Agency of the Department of Defense and was monitored by Richard W. Carman (RADC/OCSE), Griffiss AFB NY 13441 under Contract F30602-81-C-0260.

UNCLASSIFIED

SECURITY CLASSIFICATION OF THIS PAGE (When Data Entered)

REPORT DOCUMENTATION PAGE		READ INSTRUCTIONS BEFORE COMPLETING FORM
1. REPORT NUMBER RADC-TR-82-320	2. GOVT ACCESSION NO. AD-A126053	3. RECIPIENT'S CATALOG NUMBER
4. TITLE (and Subtitle) ACOSS TWELVE (Active Control of Space Structures)		5. TYPE OF REPORT & PERIOD COVERED Interim Report Aug 81 - Apr 82 6. PERFORMING ORG. REPORT NUMBER N/A
7. AUTHOR(s) Jean N. Auburn		8. CONTRACT OR GRANT NUMBER(s) F30602-81-C-0260
9. PERFORMING ORGANIZATION NAME AND ADDRESS Lockheed Missiles & Space Company, Inc. Space Systems Division, P. O. Box 504 Sunnyvale CA 94086		10. PROGRAM ELEMENT, PROJECT, TASK AREA & WORK UNIT NUMBERS 62301E C6540112
11. CONTROLLING OFFICE NAME AND ADDRESS Defense Advanced Research Projects Agency 1400 Wilson Blvd Arlington VA 22209		12. REPORT DATE December 1982 13. NUMBER OF PAGES 104
14. MONITORING AGENCY NAME & ADDRESS(if different from Controlling Office) Rome Air Development Center (OCSE) Griffiss AFB NY 13441		15. SECURITY CLASS. (of this report) UNCLASSIFIED 15a. DECLASSIFICATION/DOWNGRADING SCHEDULE N/A

16. DISTRIBUTION STATEMENT (of this Report)

Approved for public release; distribution unlimited.

17. DISTRIBUTION STATEMENT (of the abstract entered in Block 20, if different from Report)

Same

18. SUPPLEMENTARY NOTES

RADC Project Engineer: Richard Carman (OCSE)

19. KEY WORDS (Continue on reverse side if necessary and identify by block number)

Control Theory
Large Space Structure
Structural Dynamics
Flexible Vehicles
Stability Augmentation
Micro-Vibration Suppression
Low and High Authority Control

20. ABSTRACT (Continue on reverse side if necessary and identify by block number)

The objective of ACOSS is to develop and demonstrate the technology required to suppress vibrational disturbances (damping augmentation and elastic mode control) of large space structures so that they can meet the required line-of-sight and jitter control requirements. In this effort a control methodology is developed for disturbance rejection and an analysis is done for a sample surveillance structure, ACOSS-2. The work includes looking at robustness and assessing system identification methods. The

DD FORM 1 JAN 73 1473 EDITION OF 1 NOV 65 IS OBSOLETE

UNCLASSIFIED

SECURITY CLASSIFICATION OF THIS PAGE (When Data Entered)

theory is being applied to several bench top brassboards and these experiments are reported in detail. A proof-of-concept experiment will be conducted at RF tolerances and this five meter structure is reported on.

TABLE OF CONTENTS

LIST OF FIGURES

LIST OF FIGURES (Continued)

LIST OF FIGURES (Continued)

LIST OF TABLES

LIST OF TABLES (Continued)

1.0 ANALYTICAL RESEARCH FOR CONTROL METHODOLOGY DEVELOPMENT (TASK 1.0)

The discussion contained in the following sections present an overview of the activities performed on the ACOSS 12 contract. This overview is on the activities accomplished on the program through April 1982. The objective of the Task 1.0 activities are to refine and extend the analytical activities started during the Phase I and Phase IA programs at Lockheed Missiles and Space Company, Inc.

1.1 ANALYSIS OF DISTURBANCE REJECTION ON CSDL #2 (TASK 1.1)

The CSDL No. 2 model, shown here conceptually, represents a wide-angle, three-mirror optical space system, together with a line-of-sight model giving the law of displacement of the image in the focal plane when the structure deforms. The assumption is made that the mirror surfaces are simply displaced and maintain their nominal (rigid) shapes. The mirror shapes are off-axis sections of rotationally symmetric coaxial surfaces. Since the intent is to derive a first-order optical model (by neglecting the influence of light redistribution in the image), the asphericity of each mirror is disregarded.

The total structure is approximately 28 m high, has a mass of about 9,300 kg, and embodies a structural design based on realistic sizes and weights (Figure 1-1).

Draper Model Number Two had two sine disturbances. One at 10 N and 10 Hz on the top of the truss and one at 5 Hz and 20 N on the aft body. The sine disturbances are only one class of disturbance and do not fully test the theory being demonstrated. A more general model for the disturbances occurred across the many modes (Figure 1-2). The level selected was chosen on the basis of supplying wideband approximately as much disturbance energy to the system as the original two discrete systems supplied if one assumed a damping ratio of .002. The 15 Hz rolloff was selected to include more modes than previously considered. The three

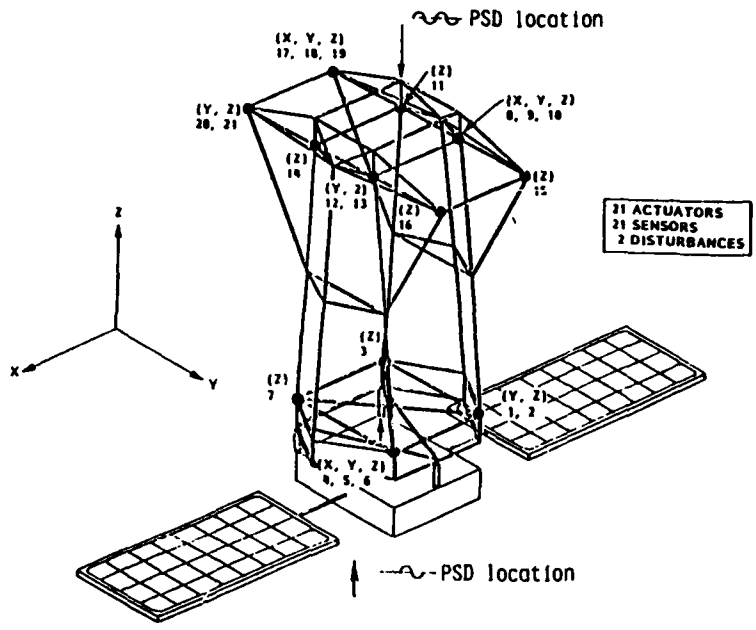

Figure 1-1 CSDL #2 - Disturbances and Actuator/Sensor Locations

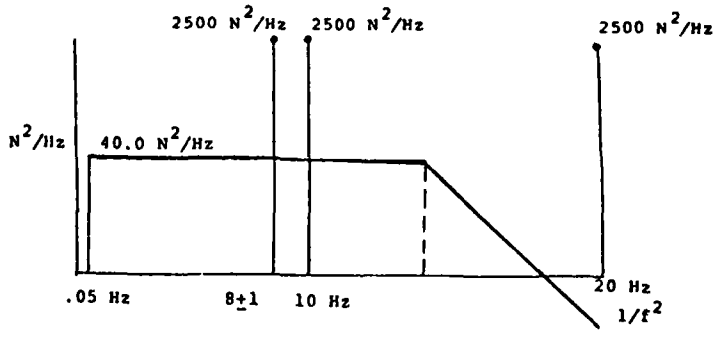

Figure 1-2 Disturbance PSD

discrete frequencies are selected to represent motors, etc. The 10 and 20 Hz frequencies were selected to present the problem of control of frequencies at multiples of each other. The 8 Hz frequency was selected to provide a beat frequency against the 10 Hz frequency that was in the structural control bandwidth. The +1 Hz on the 8 Hz frequency was to insure a mode would be directly excited by a sine source.

A preliminary selection of controls may be made based on the noise components which are most difficult to suppress in the structure. In previous work (Phase IA Final Report), the effect of sine type disturbances on the LOS was controlled by forcing the structure to vibrate in the null space of the line-of-sight metric. This required active controls to modify certain eigenvectors (mode shapes) of the open-loop system. Damping augmentation was not significant except that required to stabilize HAC spillover effects in the unmodeled plant dynamics. The new disturbance spectrum provides no new monochromatic rejection problems. Within a narrow band reduced-order model, these disturbances are suppressed as before. Coincidence with a structural mode may require some HAC modal frequency shafting which is easily accomplished since the disturbance frequency is easily identified. In the unmodeled region, a sine disturbance will generally be ignorable. If not, the system model, as it affects LOS, will have to be identified close to the disturbance frequency. This is generally straight forward. The monochromatic disturbance rejection for these new oscillators will be illustrated later in the program. The brassboard disturbance poses more severe problems. Broadband excitation means that:

- damping will provide little improvement
- reduced order models may not adequately describe propagation to the LOS
- eigenvector modification (zeros distribution) will produce little improvement

This will be illustrated now with some results for the basic damping augmentation controller. The disturbance model for the colored noise is quantified in Table 1-I.

- Disturbance is modeled as two independent colored noise sources

$$\begin{bmatrix}\dot{\nu}_1\\ \dot{\nu}_2\end{bmatrix} = \begin{bmatrix}-\beta & 0\\ 0 & -\beta\end{bmatrix}\begin{bmatrix}\nu_1\\ \nu_2\end{bmatrix} + \omega \; ; \; \omega \sim n(0, \begin{bmatrix}M & 0\\ 0 & M\end{bmatrix})$$

$\beta = 30\pi$; $M = 18000\pi$ N^2/sec

Covariance: $E(\nu\nu^T) = \begin{bmatrix}300 & 0\\ 0 & 300\end{bmatrix} N^2$

PSD: $\nu_1(\omega) = \frac{18000\pi}{\omega^2+(30\pi)^2}$ N^2-sec

- Disturbance is applied in z-direction only

- Augmented evaluation model:

$$\begin{bmatrix}\dot{x}\\ \dot{\nu}\end{bmatrix} = \begin{bmatrix}A & D\\ 0 & \equiv\end{bmatrix}\begin{bmatrix}x\\ \nu\end{bmatrix} + \begin{bmatrix}0\\ I\end{bmatrix}\omega + \begin{bmatrix}B\\ 0\end{bmatrix}u$$

$$z = [M \; 0]\begin{bmatrix}x\\ \nu\end{bmatrix}$$

Table 1-I Disturbance Model

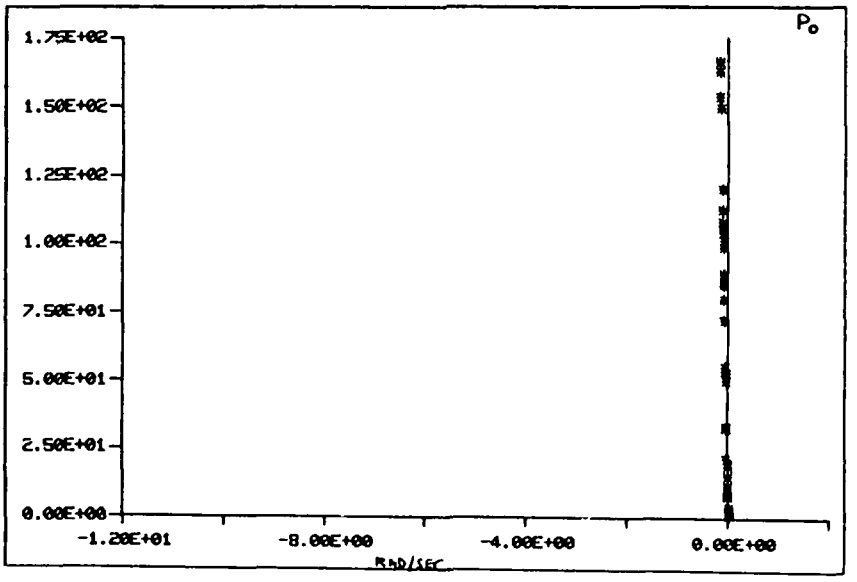

Figure 1-3 Open-Loop CSDL Evaluation Model (P_0)

The open-loop poles for the evaluation model, assuring 0.1% damping, are shown in Figure 1-3. Forty-four modes, with rigid body removed, will be assumed in the evaluations. The selection of modes will be made by using Moore's internal balancing to provide a natural ordering based on controllability-observability or disturbability-observability through the LOS measurement. Tables 1-II and 1-III give the basic characteristics and formulae for this ordering. The resulting rankings of the modes are shown in Table 1-IV. As before, stability considerations dictate that the most controllable modes be retained. The black dots indicate modes retained in the reduced order model. In Table 1-V the comparison between broadband noise effects (stochastic columns) and sine disturbances is illustrated. The broadband effects dominate and it is seen that rigid body effects are negligible in the LOS.

Reduced Order Control Design

The relevant pole constellations for the open and closed-loop reduced order models are shown in Figure 1-4. The low frequency poles are provided in a nearly constant damping ratio in closed-loop. In Figure 1-5 this controller is evaluated using the full evaluation model and, with an expanded scale near the origin, spillover is evident. Low-authority control (the same control used in Phase IA) is added to this system in Figure 1-6 (expanded scale in Figure 1-7) and the spillover problem is corrected. Using frequency shaping to limit low-frequency gain would have provided a similar result in this case, but not in general.

Performance Summary

The performance summary for the damping augmentation controller is shown in Table 1-VI for the nominal and both perturbed models. Reduction factors of about 8 are observed and this performance is clearly inadequate. As suggested earlier, damping provides only local effects on the transfer functions and broadband disturbances propagate significant energy away from the modal peaks. Disturbance accommodation, discussed in the next

(1) Stochastic Modal Cost Ranking

(2) Internal Balancing [B. C. Moore, IEEE TAC Feb. 1981]

- Def. An asymptotically stable model $\begin{Bmatrix}\dot{x} = Ax + Bu \\ y = Cx\end{Bmatrix}$ is

  Internally balanced over [0,∞] IFF

  $$\int_0^\infty e^{At} BB^T e^{A^T t} dt = \int_0^\infty e^{A^T t} C^T C e^{At} dt = \Sigma^2$$

  where $\Sigma^2 = \text{diag}\left\{\sigma_1^2\ \sigma_2^2 \ldots \sigma_n^2\right\}$ and $i>j \Rightarrow \sigma_i^2 \geq \sigma_j^2$

- Provides a natural (and unique) controllability-observability ordering criterion, but "scrambles" the states.

- For lightly-damped structural models with decoupled dynamics, internal balancing simply scales the states. Modal structure is preserved.

- Approximate formulae for $\left\{\sigma_i^2\right\}$ can be written in terms of the original model.

Table 1-II Mode Selection Criteria

$$\dot{x} = \left[\begin{array}{cc:cc:c} -2\zeta_1\omega_1 & -\omega_1^2 & 0 & & \\ 1 & 0 & & & \\ \hdashline & & -2\zeta_2\omega_2 & -\omega_2^2 & \\ 0 & & 1 & 0 & \\ \hdashline & & & & \ddots \end{array}\right] x + \left[\begin{array}{c} b_1 \\ 0 \\ \hdashline b_2 \\ 0 \\ \hdashline \vdots \end{array}\right] u + \left[\begin{array}{c} d_1 \\ 0 \\ \hdashline d_2 \\ 0 \\ \hdashline \vdots \end{array}\right]$$

$$y = \left[b_1^T\ 0\quad b_2^T\ 0\quad \ldots\right] x \quad \text{(sensors)}$$

$$z = \left[0\ m_1\quad 0\ m_2\quad \ldots\right] x \quad \text{(LOS)}$$

- Controllability - Sensors: $\sigma_i^2 \approx \dfrac{b_i b_i^T}{4\zeta_i\omega_i}$

- Controllability - LOS : $\sigma_i^2 \approx \dfrac{[(b_i b_i^T)(M_i^T m_i)]^{\frac{1}{2}}}{4\zeta_i\omega_i^2}$

- Disturbability - LOS : $\sigma_i^2 \approx \dfrac{[(d_i d_i^T)(m_i^T m_i)]^{\frac{1}{2}}}{4\zeta_i\omega_i^2}$

Table 1-III Application of Internal Balancing to Lightly-Damped Structural Model

Controllability -LOS	Disturbability -LOS	Stochastic "Modal-Cost"
7 •	7 •	21 •
21 •	21 •	7 •
8 •	13 •	12 •
12 •	16 •	13 •
13 •	10 •	16 •
17 •	14	14
10 •	8 •	24
30 •	24	30 •
47	22	22
46	30 •	10 •
35	17 •	50
39	50	37
45	37	35
37	35	8 •

Selection:

- First eight contr.-LOS modes
- Add mode 16 because of high disturbability

Table 1-IV Ranking of Modes (Neglecting Rigid Body)

MODE	SINE LOS	STOCHASTIC MODAL COST	STOCHASTIC MODAL COST WITHOUT RIGID BODY
4	136.401	49026.975	0.000
5	109.737	39684.188	0.000
6	0.000	0.000	0.000
7	49.086	94659.768	94554.114
8	4.120	3227.033	3256.289
9	0.166	76.291	95.850
10	9.455	5280.456	5248.095
11	1.358	490.972	490.496
12	92.663	22432.584	22424.285
13	74.429	17837.036	17842.280
14	126.502	9745.869	9746.603
15	1.487	107.085	107.008
16	194.843	12924.866	12925.704
17	57.241	2583.097	2583.419
18	0.079	3.413	3.832
19	0.016	1.101	1.175
21	4780.464	128053.989	128054.154
22	313.515	5568.336	5568.472
23	2.662	43.700	43.806
24	614.836	8637.361	8637.287
25	0.000	0.013	0.010
26	29.502	149.357	149.427
27	0.012	0.017	0.005
28	6008.083	876.149	876.190
29	2440.540	1004.205	1004.291
30	9323.458	5758.592	5758.520
31	11.957	5.761	5.900
32	0.044	1.040	1.038
34	251.899	293.718	293.606
35	2313.826	3976.443	3976.349
36	696.705	1338.458	1338.386
37	2149.369	4252.422	4252.530
38	245.698	515.033	515.062
39	465.489	950.199	950.300
40	297.456	591.673	591.769
41	445.360	829.427	829.365
42	476.921	848.065	847.937
43	982.472	1559.022	1558.907
44	447.167	563.091	563.234
45	3431.405	1825.390	1825.509
46	51.517	74.308	74.486
47	554.378	821.245	821.131
48	218.905	370.473	370.636
50	2448.200	4353.281	4353.311

Table 1-V Modal Costs

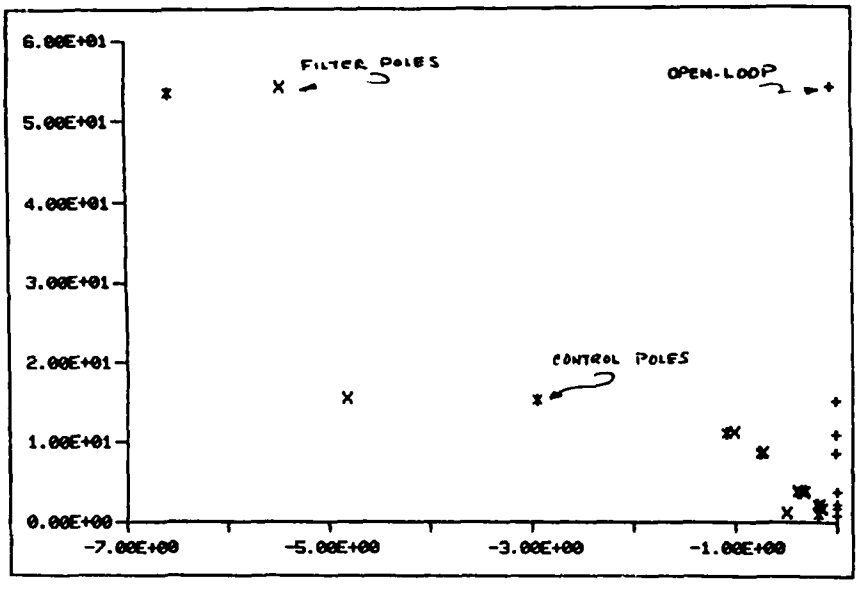

Figure 1-4 Reduced P_0 Design Model

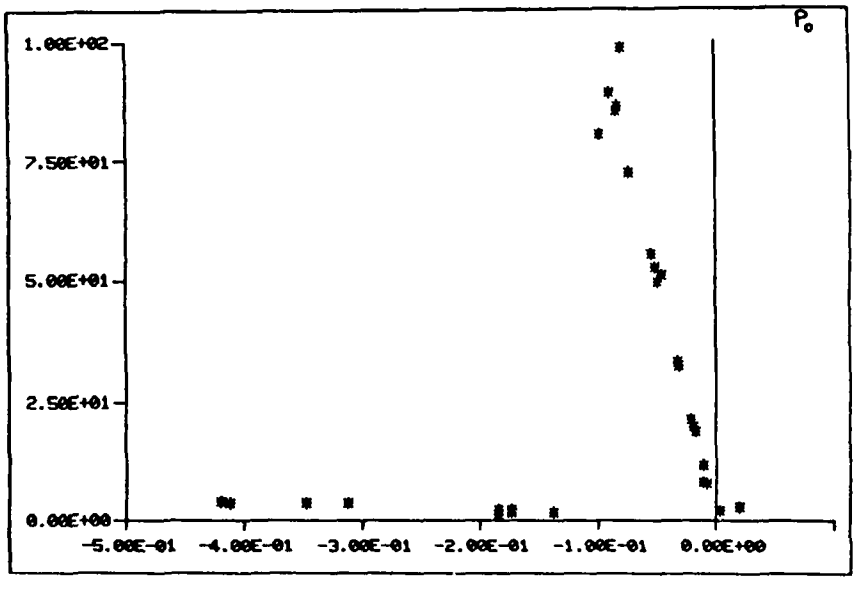

Figure 1-5 High-Gain HAC Evaluation (Expanded Scale)

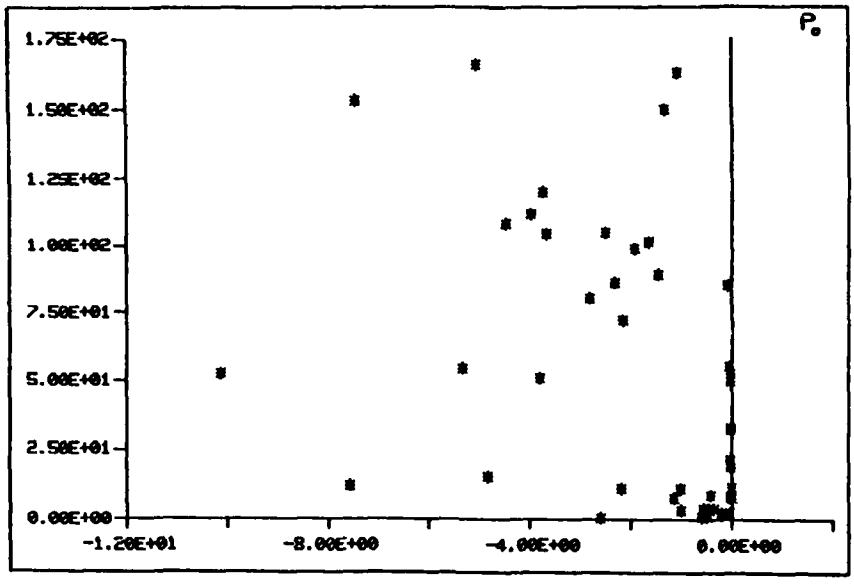

Figure 1-6 High-Gain HAC + LAC Evaluation (P_0)

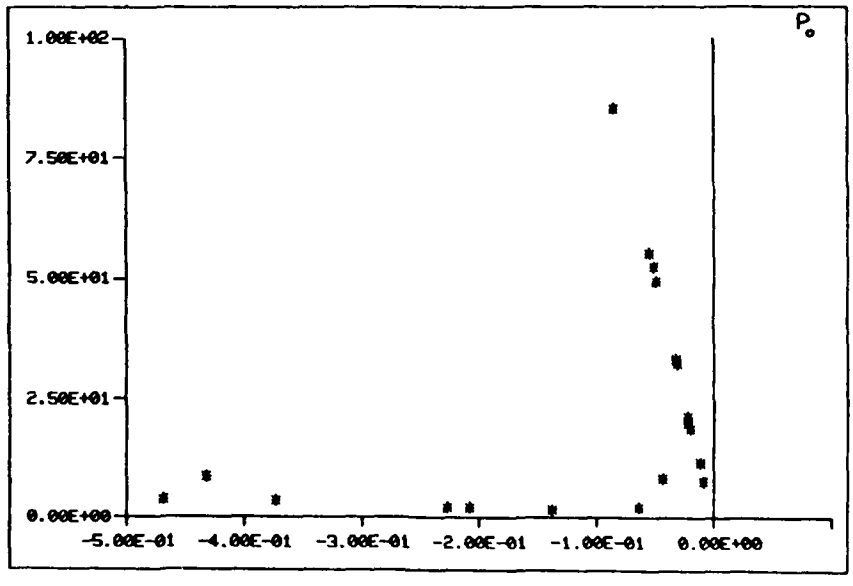

Figure 1-7 High-Gain HAC + LAC (Expanded Scale)

	P0		P2		P4	
	Open Loop	Closed Loop	Open Loop	Closed Loop	Open Loop	Closed Loop
RMS LOS x (n RAD)	28,110	11,940	27,750	11,110	30,500	12,490
RMS LOS y (n RAD)	160,900	17,290	157,700	16,340	156,900	16,860
Total RMS LOS (n RAD)	163,300	21,020	160,000	19,760	159,800	20,980
Control Effort (N)	0	18.74	0	17.24	0	18.26

- Damping augmentation is ineffective against broadband noise.

Table 1-VI Performance Analysis

TD meeting, will alter these conclusions somewhat at the price of a more complex control. Adaptive methods will be necessary to identify the contributions of the unmodeled plant dynamics transmission to the LOS. This work will be performed in conjunction with tests to reduce the number of actuators currently used on CSDL #2.

1.2 CONTROLLER ROBUSTNESS INVESTIGATION (TASK 1.2)

The principal objectives are described in Table 1-VII. While system stability is important, performance sensitivity to parameter uncertainty for high performance missions is a much more significant issue. In particular, what must be determined is how much performance is lost to insure stability and acceptable performance sensitivity. Some systems/missions may require identification or adaptive strategies to reduce the risk of losing the mission. At the core of these problems is the difficulty of selecting analysis and synthesis tools to determine robustness properties. Toward this end, analysis tools like generalized Nyquist criteria and angular value decomposition of the return difference matrix will be used to evaluate reduced-order designs. These techniques are known to produce only conservative evaluations of system sensitivity but as yet have not been used on space structure system examples.

The most fundamentally important issue, however, is the designer's access to synthesis tools which allow him to synthesize robust controls. Many techniques have been proposed but only two will be advocated for now, i.e.:

- frequency shaping
- adaptive methods

Direct sensitivity minimation via the usual gradient searches is complex, computationally expensive and usually produces only small improvements. Fixed gain and adaptive controls can be tailored using frequency shaping techniques so that high loop gains are present only in regions of high modal fidelity (either identified or known a priori).

OBJECTIVE: Develop Synthesis/Analysis techniques to improve/define system robustness properties with respect to:

I. Stability
- Excessive perturbation of unmodeled-pole locations (spillover) } MODEL ERROR
- Parameter sensitivity of controlled/modeled poles
- Gain/phase/frequency margins

II. Performance
- Performance metric sensitivity to:
  - disturbance parameters (modeled and unmodeled)
  - identified modes
  - unidentified modes
- Performance/robustness trade-off

In general, the second class of issues is more important than the first.

➡ General objective is to understand the limitations imposed by model/disturbance uncertainty on closed-loop performance

Table 1-VII Controller Robustness Investigation

- Performance Criterion
  - Stability
  - Zero Asymptotic Error
  - $\underset{\substack{\text{plant} \\ \text{variations}}}{\text{MIN MAX}} \{J_{control}\}$
  - $\underset{\substack{\text{plant} \\ \text{variations}}}{E} \{J_{control}\}$
- Specification of Variations
  - Parameter variations in design model (too restrictive)
  - Frequency-domain specifications (easy to use but pessimistic)
  - Function space specifications (too analytical, useable with frequency domain specs.)
  - Probability distributions (computationally expensive)

Table 1-VIII Robustness Definitions

Possible definitions of robustness are provided in Table 1-VIII with comments on specification of performance and parameter variations. Monte Carlo type solutions and probability distribution will be avoided for the present since these techniques are computationally expensive and reduce physical understanding of the problem.

Analysis tools such as the singular value decomposition of the return difference matrix, illustrated in Figure 1-8, can provide stability boundaries (conservative) analysis for given system designs. What is needed, however, are synthesis tools which allow robustness problems to be corrected.

Full-state loop transfer function recovery has been suggested by Stein as a method to increase loop gain sufficiently to eliminate parameters sensitivity. As shown in Figure 1-9 and Table 1-IX, however, this procedure attempts to invest the system dynamics and provides no gain stabilization in the region of unmodeled plant dynamics.

Frequency shaping avoids these problems by not exploiting modeling deficiencies. Characteristics are listed in Table 1-X. For the two-mode example developed earlier, the gain reduction achieved with frequency shaping in the region of the unmodeled mode at 5 rad/sec is illustrated in Table 1-XI and Figure 1-10.

The highest levels of robustness will be attainable with adaptive mechanizations. To illustrate this, disturbance rejection (of a sinusoidal) is now shown for a helicopter example. This technique will be used subsequently on the CSDL broadband vibration problem. The technique exploits the characteristics of self-tuning regulators.

The objective of the time-domain self-tuning regulator is to develop a time-domain feedback control design approach in which the helicopter model at the vibration frequency can be continuously identified. Even though the time-domain frequency-shaped formulation is robust with respect to changes in model form, the associated state variable model is difficult to identify in real-time, should this become necessary.

- Stability Robustness:

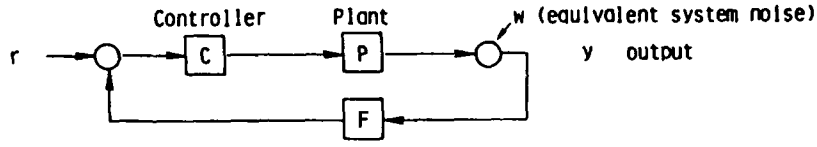

$$(P.C.F.)_{perturbed} = (1 + \Delta(PCF))\ PCF$$

Δ: multiplicative form of uncertainty

$$\sigma_{min}(\Delta(PCF)) < \sigma_{min}(1 + (PCF)^{-1}),\ \forall\omega$$

then the perturbed system is stable, when unperturbed system is stable

- Stability does not guarantee performance improvement

Figure 1-8 Singular Values of Return Difference Matrix

$$\dot{x} = Fx + Gu + w \ ; \quad y = Hx + v$$

$$\phi(s) \equiv (sI - F)^{-1} \ ; \quad u = C\hat{x}$$

K = Filter gains

- Make $H\phi G$ and $C\phi G$ square via zero rows/columns
- Use $E(ww^T) = [M_0 + q^2 GG^T]\ \delta(t-\tau)$

  $E(vv^T) = M_0\ \delta(t-\tau)$
- Let $q \to \infty$
- Effectively inverts reduced-order plant dynamics (pole-zero cancellation)
- Does not control gain in model uncertainty region

Figure 1-9 Full-State Loop Transfer Recovery

	q = 10	q = 100
Filter poles	- 0.10 -10.8	- 0.01 -101
Controlled mode	- 0.48 ± j.85	- 0.48 ± j.84
Unmodeled mode	0.38 ± j 4.9	0.45 ± j 5.05

- Loop gain is too high at 5 rad/sec

Table 1-IX Loop Transfer Recover on 2-Mode Example

- Frequency weighted penalties can be imposed for:
  - state and measurement noise estimates
  - states and controls (control problem)
  - likelihood function (identification)
  - fault detection (likelihood ratio)
- Loop gain can be controlled in regions of uncertainty
- Factor A & B in $J = \int_{-\infty}^{\infty} [x^*(j\omega)A(j\omega)x(j\omega) + u^*(j\omega)B(j\omega)u(j\omega)]d\omega$

  to get augmented time domain controller
- Refer to 2-mode example in previous section

Table 1-X Robustness Improvements Via Frequency-Shaping

	Basic LQG:	Frequency-Shaped
Unmodeled mode	0.0164 ± j 4.9084	-0.0262 ± j 5.0002
Filter poles	-0.4049 ± j 0.8627	-0.4232 ± j 0.8952
Controlled poles	-0.6466 ± j 0.8512	-0.7018 ± j 0.5139
Frequency shaping	-	-0.3839 ± j 1.0957

Table 1-XI Comparison of Closed-Loop Modal Shift

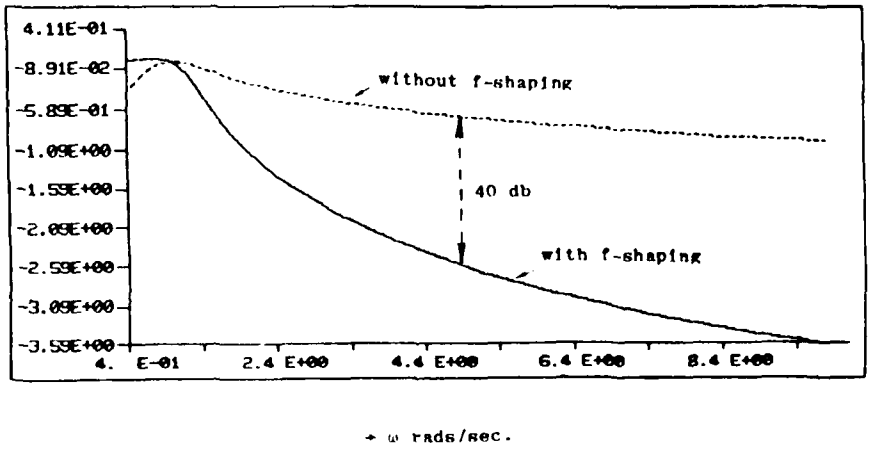

Figure 1-10 $\text{Log}_{10}\ (L(1+L)^{-1})$ State-Feedback Only

The proposed approach can be shown to be convergent for any noise level, because it does not suffer from a leakage problem associated with Fourier transformed data used in the multicyclic approach.

Preliminary research conducted to date indicates that this approach can combine the best features of the multicyclic frequency-domain and the frequency-shaped time-domain methodologies. The identification part of the approach continuously updates a time-domain model, much like the multicyclic approach. The only difference is that the proposed approach can update the model at each measurement point. The control input is also computed at each point, leading to fast response for changes in helicopter dynamics or vibration level. The time-domain self-tuning regulator also has guaranteed convergence characteristics irrespective of the measurement noise and process noise levels, if the helicopter dynamics do not change too rapidly.

The self-tuning regulator concept can be applied to the vibration control problem in the time-domain because of a recent development in which a frequency-shaped error criterion can be minimized instead of the mean-square error. This development is critical because the standard self-tuning regulator as proposed by Astrom cannot be used successfully to control helicopter vibration in a time-domain formulation, because of the need to focus on the response at the vibration frequency.

The following tables and figures show the theoretical development of the approach, i.e., the extensions to the self-tuning regulator to incorporate a frequency-shaped error criterion. The results are applied to a simplified simulation of a six-bladed rotorcraft, in high noise environment and when there is an unmodeled mode close to the vibration frequency.

The results for the self-tuning regulator are illustrated in Tables 1-XII and 1-XIII and Figure 1-11. Identification and control adaption is complete (steady state) in about 1 sec.

$$\dot{x} = Fx + Gu$$

$$y = Hx$$

with $x^T = [w \ \xi \ \dot{\xi}]$

where w is the vertical speed in ft/sec.

ξ is a structural mode closed to the vibration frequency

u is the collective pitch control in degrees

$$F = \begin{bmatrix} -.5034 & -8.69\times10^3 & -67.4 \\ 0 & 0 & 1 \\ .7116 & -5.1372\times10^3 & -6.8 \end{bmatrix} \qquad G = \begin{bmatrix} -16.92 \\ 0 \\ 13.2 \end{bmatrix}$$

$$H = [\ 1 \quad 0 \quad 0]$$

Sample rate of 180 Hz gives

$$\frac{y}{u} = \frac{-.1294Z^2 + .1863Z - .0903}{Z^3 - 2.8045Z^2 + 2.7661Z - .9601}$$

Table 1-XII 3-Mode Example - Model (Reduced)

$$y = \frac{-.1294Z^2 + .1863Z - .0903}{Z^3 - 2.8045Z^2 + 2.7661Z - .9601}u + \frac{Z^3 - .1Z^2}{Z^3 - 2.8045Z^2 + 2.7661Z - .9601}v + \delta_{vib}$$

v is white noise

δ_{vib} is sinusoidal (18 Hz)

unmodeled pole-pair at 27 Hz

The frequency-shaping filter was chosen to be

$$\frac{\gamma(Z)}{\Phi(Z)} = \frac{Z^2 - 1.60185Z + .9801}{Z^2 - 1.61803Z + 1}$$

Sensor noise level selected to produce 50% of steady-state error

Table 1-XIII Propagation of Noise & Vibration

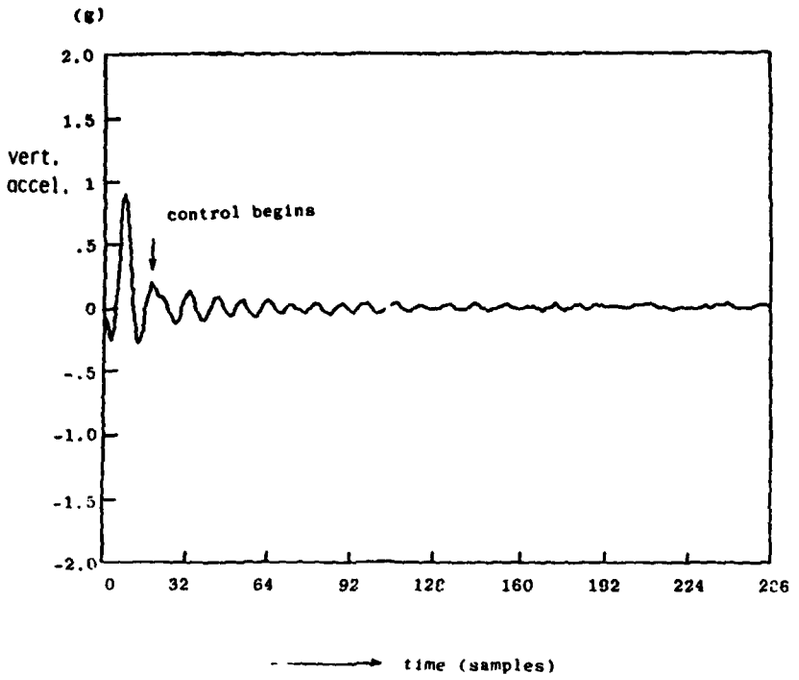

Figure 1-11 Adaptive Control with Unmodeled Pole Pair

Robustness Investigation Program

The tasks needed to complete robustness techniques evaluations are listed below. Other evaluations will be included as appropriate.

1. Refine parameter sensitivity (model error) definition and synthesis methods.
2. Perform parameter sensitivity study on CSDL strawman model for:
   a. Evaluate singular value analysis for practical parameter variations.
   b. Select performance variation criteria and evaluate singular value decomposition/robustness properties.
   c. Evaluate limits of adaptive disturbance accommodation
   d. Evaluate robustness/performance trade-off
3. Assessment of adaptive control strategies against parameter variations studies in Task 2.
   a. Model Structure changes
   b. Lattice form mechanization

1.3 SYSTEM IDENTIFICATION METHODS ASSESSMENT (TASK 1.3)

Because the damping ratios of structural modes are required with high precision and the data is often noisy, advanced identification techniques are desired. Currently used real-time techniques are highly suboptimal (e.g., least-squares fit to transfer functions, random decrement signatures, and Pancu-Kennedy plots).

The estimated parameters must be updated at regular intervals to continuously track any changes in modal characteristics. Thus, a recursive technique is desirable. The traditional frequency-domain fitting method is illustrated in Table 1-XIV.

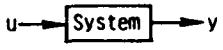

$$\frac{\hat{y}(jw)}{\hat{u}(jw)} = \hat{H}(jw)$$

Least-squares fit to $\hat{H}(jw)$ gives parameters.

Chirp input

Table 1-XIV Traditional Frequency-Domain Method

ALGORITHM	ADVANTAGES	DISADVANTAGES
Frequency Domain Instrumental Variables	•Always converges •Requires no starting values •Data can be averaged for use with low signal-to-noise ratio •Number of active modes can be easily determined	•Not minimum variance •Can only be block recursive •Requires solution to a polynomial equation •Difficult to make it robust
Recursive Maximum Likelihood	•Minimum variance •Always converges •Easy to incorporate robustness against data dropouts	•Requires solution to a polynomial equation to compute damping ratios and frequencies •Discrete ARMA leads to poles near the unit circle

Table 1-XV Investigative Techniques

System identification methods development will follow this sequence of steps:

- Establish data base for plate and wheel models in open and closed loop cases
  - high-q and low-q modes
- Establish FFT baseline analysis
- Test recursive maximum likelihood and instrumental variables software against data bases
- Refine algorithms and evaluate limitations

Currently, data bases are being established for the plate and wheel models, some of which will be discussed below. Although instrumental variables has already been tested in the POC lab, results illustrated here will emphasize recursive maximum likelihood techniques which are applicable in on-board system ID situations. The two techniques are compared in Table 1-XV.

The least-squares method gives biased estimates of parameters when the input measurement is contaminated by noise. The instrumental-variables technique was developed to minimize the bias in estimates. In addition, unlike least-squares, the instrumental-variables method does not require solution to a nonlinear programming problem. The instrumental-variable estimates are, therefore, obtained in a single step.

Recursive prediction error methods based on discrete ARMA models update estimates at each data point. The algorithms include recursive maximum likelihood, recursive least squares, recursive instrumental variables, and extended Kalman filter (corrected). These have been used successfully in signal processing and process control and monitoring applications. The RML method was an autoregressive moving average model with exogenous inputs (ARMAX) of the form

$$A(q^{-1})y = B(q^{-1})u + C(q^{-1})v$$

such that polynominals are then selected to match the output data y, where u is the system input and v are the innovations. The asymptotic properties are the same as batch maximum likelihood.

The basic results include the following characteristics:

- **Comparison with frequency domain method**
- **Nonlinearity in actuators observable in time history**
- **Closed-loop vs open-loop for attitude controller**
- **High damping ratio synthetic data results**
- **Identification model selected for 10 modes and 8 modes (20th and 16th order polynominals)**

FFT computations are displayed to indicate the poor signal to noise characteristics associated with the square-wave excitation. Curve fitting is extremely difficult in these cases.

The time response data in some cases displays non-linear damping characteristics believed to be due to the PPM actuator behavior.

High modal damping ratio tests (synthetic results) were created from analytical plate models since actual modal control data is not yet available.

The plate sensor and actuator locations are shown in Figure 1-12. The velocity measurements used in the identification are obtained by integrating the accelerometer outputs 1 and 2. The CEM actuator (5) is used to excite the specimen. The FFT for the square wave excitation is shown in Figure 1-13 and indicates why this signal provides poor excitation of the modes to be identified.

Principal measurements for system ID were the two accelerometer outputs integrated to obtain velocity of the plate surface. These signals are shown in Figure 1-14 with a zero shift so that both are visible. In Figure 1-15 these signals are compared again for the closed-loop attitude controller.

Open and closed-loop FFT's of the velocity measurements in Figure 1-16 show damping changes for the closed-loop. Note that the attitude controller destabilizes this plant. Signal-to-noise, however, makes damping ratio evaluation from the FFT difficult.

SENSORS

①, ② : INERTIAL SENSING/ ACCELEROMETERS (1 D.O.F. Z-MEASUREMENT)

③, ④ OPTICAL SENSING/MIRRORS
⑤, ⑥ (2 D.O.F. $\theta_{x'}$, $\theta_{y'}$ ANGULAR MEASUREMENT

(x', y') ARE 45° W.R.T. (x, y)

⑦–⑩: MICROPHASE OPTICAL SENSOR (Z DISPLACEMENT)

ACTUATORS

A_1, A_2 : PIVOTED PROOF-MASS

A_3, A_4, A_5 : CONTACTLESS ACTUATORS (5 MAY BE USED TO SIMULATE DISTURBANCES)

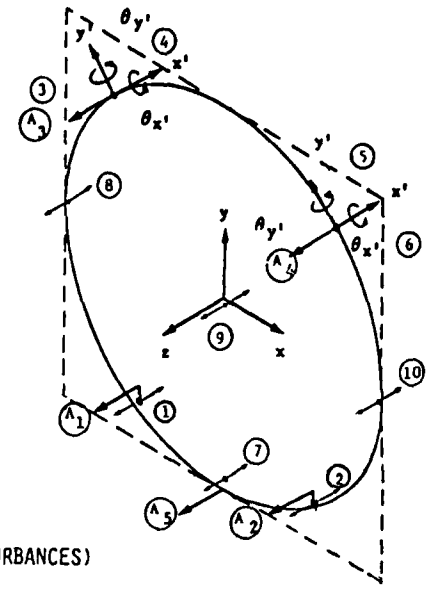

Figure 1-12 Plate Experiment Sensors and Actuators

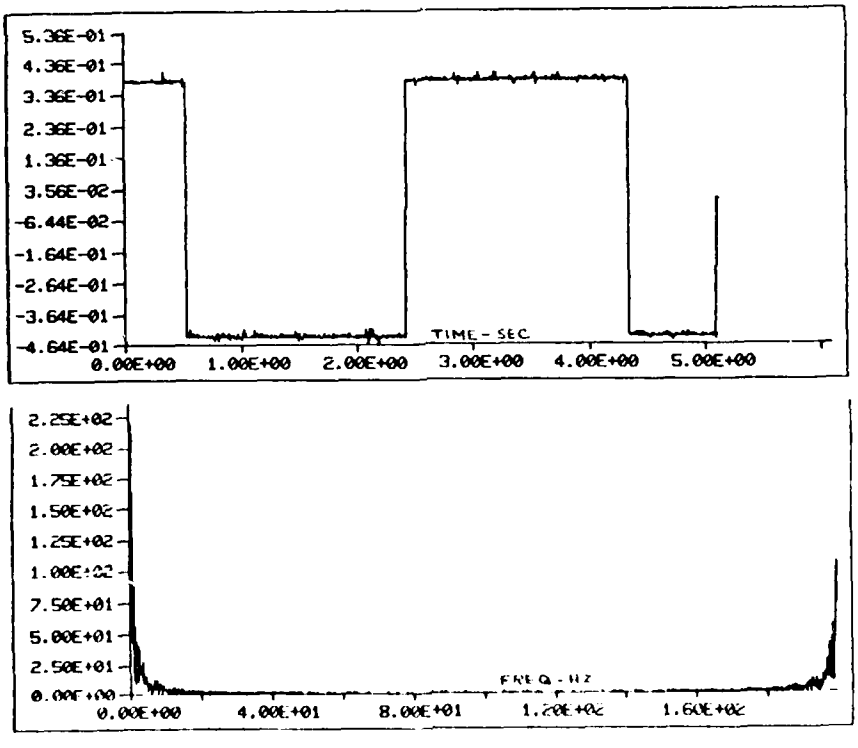

Figure 1-13 Open-Loop Input and Spectrum for Plate Identification

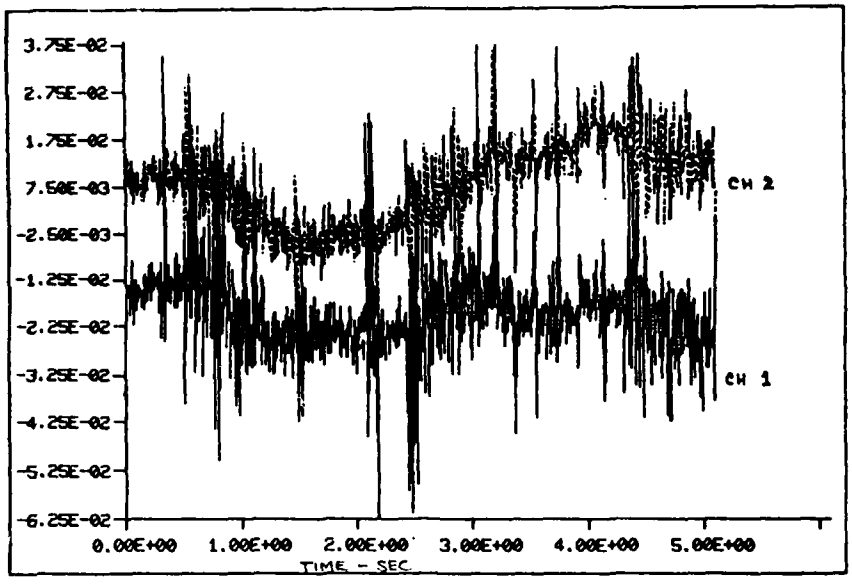

Figure 1-14 Plate Open-Loop Velocity Measurements

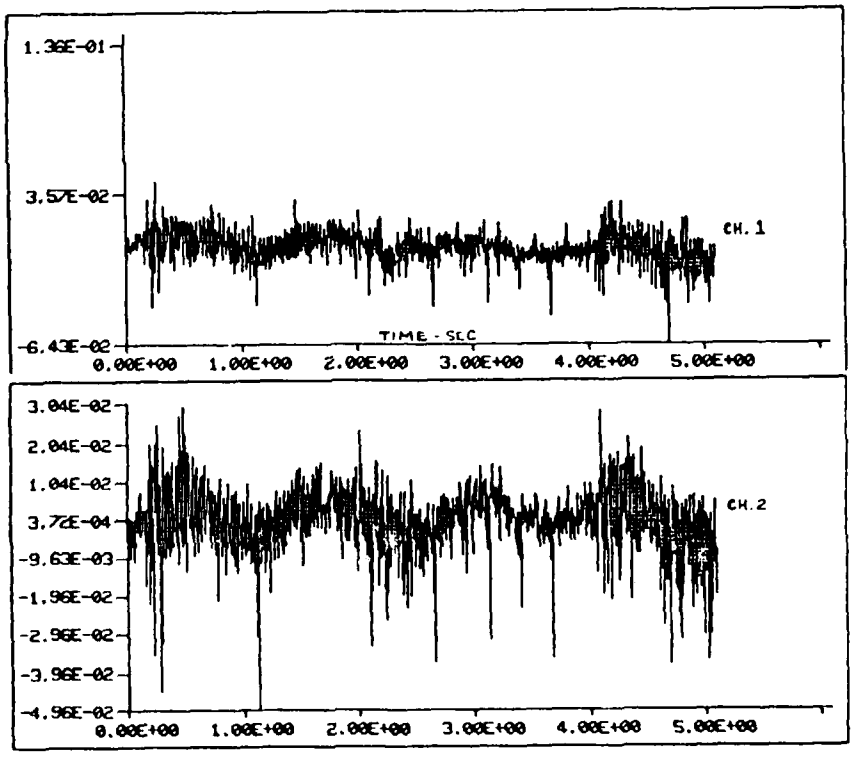

Figure 1-15 Attitude Control Closed-Loop Velocity Measurements

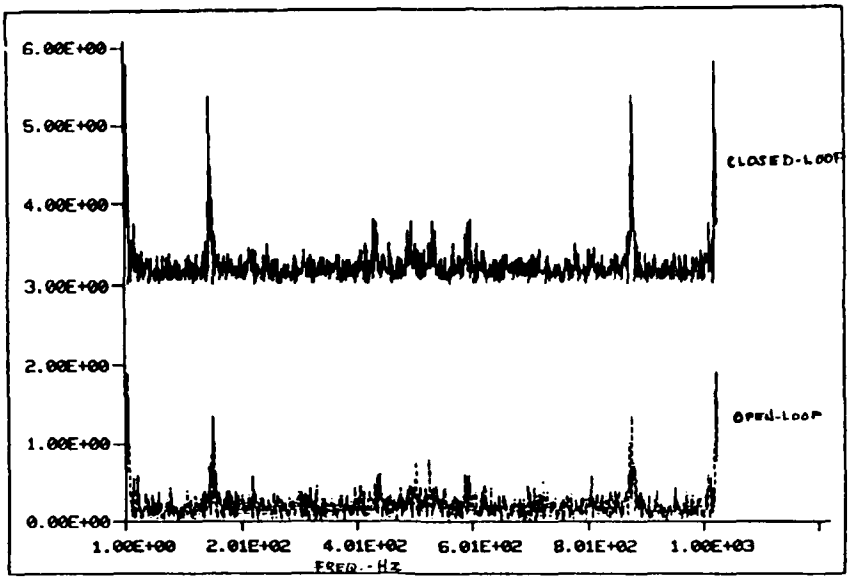

Figure 1-16 Velocity FFT Comparison (Ch. 1)

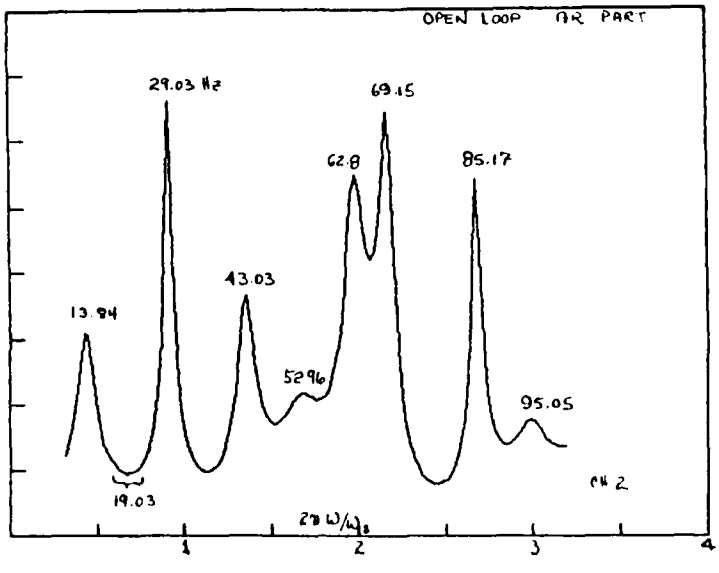

Figure 1-17 Open-Loop 20th Order ID (Poles Only)

Using RML techniques and a 25th order model, the open-loop transfer function reconstruction is shown in Figure 1-17 and 1-18. The effect of the zeros is quite pronounced, as shown in Figure 1-18 for the complete numerator and denominator dynamics.

In Figure 1-19 damping ratio is plotted vs modal frequency for some of the higher frequency modes. Variations from about 30% to nearly undamped are observed. All modeled modes and damping ratios are shown.

The effects of changing model order are illustrated in Table 1-XVI. For high q modes, damping ratio estimates are sensitive to model order as expected. Some form of automatic model structure determination will be required to obtain high accuracy for these estimates.

For modal control situations, synthetic data was created by exciting the plate analytical model and then identifying the appropriate closed-loop system. The control attempted to left-shift the open-poles of the plate. The pole-zero map is shown in Figure 1-20.

Some basic conclusions may now be drawn before proceeeding to further data processing on all experiments:

- RML provides precise estimation of frequency and damping ratios with greatly reduced information (over traditional frequency-domain methods) for plate systems.
- Actual evaluation for closed-loop modal control on plate is required.
- Further tests of technique should be performed on wheel structure and POC.
- Assessment of automatic structure determination is required.

1.4 DIGITAL CONTROLLER CHARACTERISTICS & IMPLEMENTATION (TASK 1.4)

Difficulties experienced in ACOSS Phase IA with digital implementation are addressed in this task. In particular, achieving high sample rates has been difficult for multivariable controllers. New architectures,

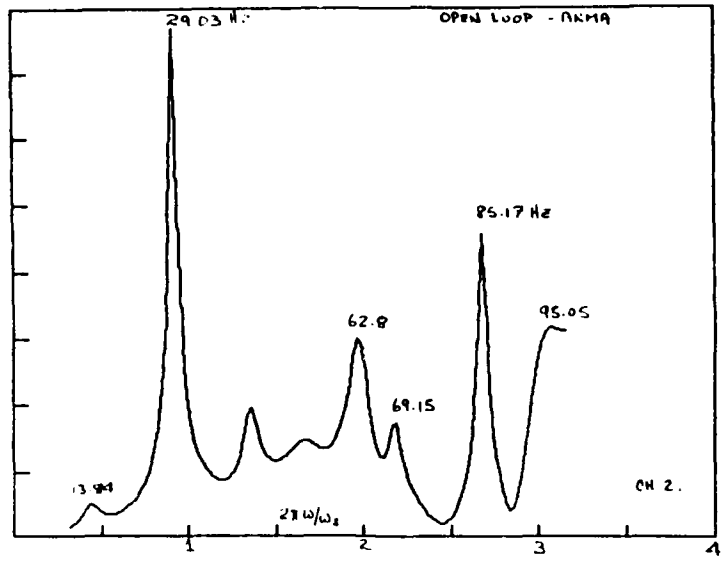

Figure 1-18 Open-Loop 20th Order ID (Poles & Zeros)

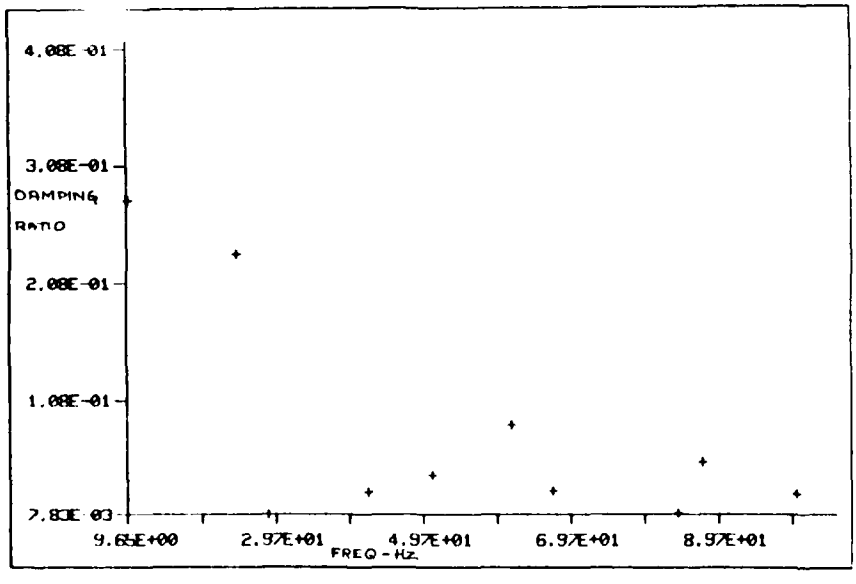

Figure 1-19 Closed-Loop Damping Ratio vs Modal Frequency

Open-Loop 16th Order Model	
Frequency (Hz)	Damping
28.76	0.0228
85.45	0.0072
43.06	0.0174

Open-Loop 20th Order Model	
Frequency (Hz)	Damping
29.02	0.0224
85.17	0.0092
43.0	0.0333
53.	
69.15	

- Damping ratio estimates sensitive to model order for high Q modes

Closed-Loop 20th Order Model	
Frequency (Hz)	Damping
28.62	0.0078
84.09	0.0092
42.02	0.0267

Table 1-XVI Comparison of Damping Ratio vs Model Order

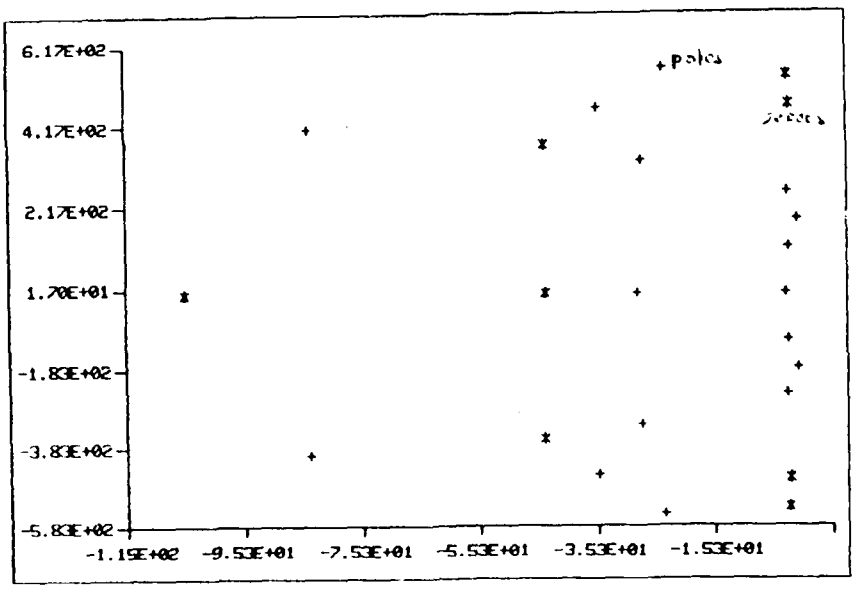

Figure 1-20 Identified Synthetic Poles & Zeros

discussed near the end of this section, will remove sampling rate constraints, but in so doing, raise the issue of filter stability vs word-length. These issues are discussed first. The basic tasks are listed below.

Task Objectives for Implementation Issues

- Word length and algorithm selection for (status: complete)
  - Minimum pole shift (robustness)
  - Mechanization stability
- Sample rate selection (status: complete)
  - Constraints imposed by stability
  - Constraints imposed by architectures
  - Architecture assessment/memory requirements
- Requirement for anti-aliasing filters (status: complete)
- Other investigations (status: research continuing)
  - Quantization effects and controller roughness
  - Throughput capacity and efficiency
  - Flexibility, fault-tolerance
  - Emulation of large spacecraft model

Multivariable Flight Control

Multivariable control methods have been highly successful for designing complex control systems for multi-input/multi-output systems. To apply multivariable control methods to flight control, the aircraft is generally represented by the equations of Table 1-XVII.

Multivariable control design is based on the quadratic cost functional shown in the table which produces the closed-loop feedback control law.

When the state x is not measured, x must be estimated from sensor outputs using the Kalman filter also shown in the table.

MULTIVARIABLE CONTROLLER EQUATIONS

State and Measurement Equations:	$\dot{x} = Fx + Gu + w$	
	$y = Hx + v$	
Control Design:	$J = \int_0^T [x^T Ax + u^T Bu]\, dt$	penalty functional
	$u = Cx$	control structure
	$SF + F^T S + A - SGB^{-1}G^T S = 0$	steady-state control gains
	$C = -B^{-1}G^T S$	
Filter Design:	$J = \int_0^T [w^T Qw + v^T Rv]\, dt$	noise covariances (weightings)
	$\dot{\hat{x}} = F\hat{x} + Gu + Kv$	filter structure
	$v = y - H\hat{x}$	
	$FP + PF^T + Q - PH^T R^{-1} HP = 0$	steady-state filter gains
	$K = PH^T R^{-1}$	

Table 1-XVII Selection of Control Algorithm Form

Kalman Filter: $\hat{x}_{k+1} = \Phi \hat{x}_k + \Gamma u_k + K[y_k - H \hat{x}_k]$

Control Law: $u_k = -C \hat{x}_k$

where Φ and Γ are discrete versions of F and G.

- Implementation Equation

$$\left(\begin{array}{c} \hat{x}_{k+1} \\ \hline u_k \end{array}\right) = \underbrace{\left[\begin{array}{c|c} F_{11} & F_{12} \\ \hline F_{21} & F_{22} \end{array}\right]}_{\text{control design matrix}} \left(\begin{array}{c} \hat{x}_k \\ \hline v_k \end{array}\right)$$

where $F_{11} = \Phi - KH - \Gamma C$, $F_{12} = K$, $F_{21} = -C$ and $F_{22} = 0$

Table 1-XVIII Steady-State LQG Controller Form

In the steady-state, the control and filter gains are constant and can be solved off-line for C and K. C and K can then be used to compute u and $\hat{x}$ in real time. Therefore, the real time calculations required to implement a steady-state multivariable controller are given in Table 1-XVIII.

The real time implementation can be performed by analog or digital circuits. However, the digital implementation is often more flexible since it can be easily modified.

By examining the steady-state controller equations it is clear that only matrix-vector multiplication is required for implementation. The matrix elements, which are constant in the steady-state designs, can be stored in memory for each flight condition. These observations form the basis for the architecture described later.

Stability Analysis

Because of modeling uncertainties, it is important to examine the margin of stability associated with the computations. Figure 1-21 gives a geometric interpretation of a stability margin in the z-plane. $|z|$ represents the magnitude of poles of H(z) and $|\Delta z|$ is the distance from $|z|$ to the edge of the unit circle. The magnitude of $|\Delta z|$ is dependent on a number of factors such as modeling uncertainties and finite wordlength considerations. From an analysis viewpoint, it is convenient to lump these considerations into a perturbation of F_{11} and analyze the stability of the eigenvalues of $F_{11} + \Delta F_{11}$.

If F_{11} is perturbed to $F_{11} + \Delta F_{11}$, then the corresponding change in the eigenvalues of F_{11}, can be estimated from the formula shown in Table 1-XIX.

Wordlength Considerations

The formula in Table 1-XX represents an effective numerical test for rapidly determining the minimum number of bits required to implement a

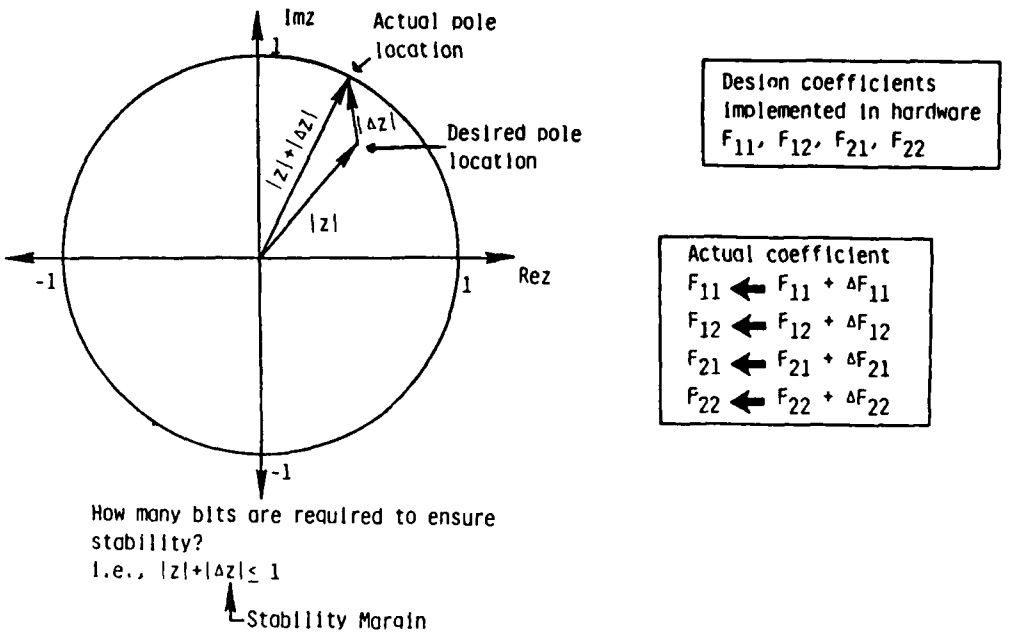

Figure 1-21 Word Length Effect on Coefficient Perturbation and Stability

For the discrete controller

$$\hat{x}_{k+1} = F_{11}\,\hat{x}_k + F_{12}\,y_k$$

$$U_k = F_{21}\,\hat{x}_k$$

If $F_{11} \rightarrow F_{11} + \Delta F_{11}$, then the change in the eigenvalues of F_{11} are given by Jacobi's formula:

$$\Delta\lambda_i = v_i^T \Delta F_{11} \Delta U_i \qquad i = 1,2,\ldots,n$$

where U and v are the right and left eigenvectors, respectively, of F_{11} and $v_i^T U_i = 1$.

For stability in z-plane,

$$|\lambda_i + \Delta\lambda_i| \leq |\lambda_i| + |v_i^T \Delta F_{11} U_i| \leq 1$$

$$|v_i^T \Delta F_{11} U_i| \leq \underbrace{1 - |\lambda_i|}_{\text{Stability Margin}}$$

Table Table 1-XIX Eigenvalue Perturbation and Stability Condition

- Perturbation in F_{11}

  $F_{11} \leftarrow F_{11} + \Delta F_{11}$ where $||\Delta F_{11}||_\infty \leq \frac{m}{2} 2^{-b}$

  where b is the number of bits, and n is the system order

- Stable Control Computations Require

  $$b = \left\lceil -(1 + \log_2 ((1-\lambda_{max})/n)) \right\rceil \geq 0$$

  where $\lambda_{max} = \max_{1 \leq i \leq n} |\lambda_i|$

Table 1-XX Minimum Number of Bits to Insure Controller Stability

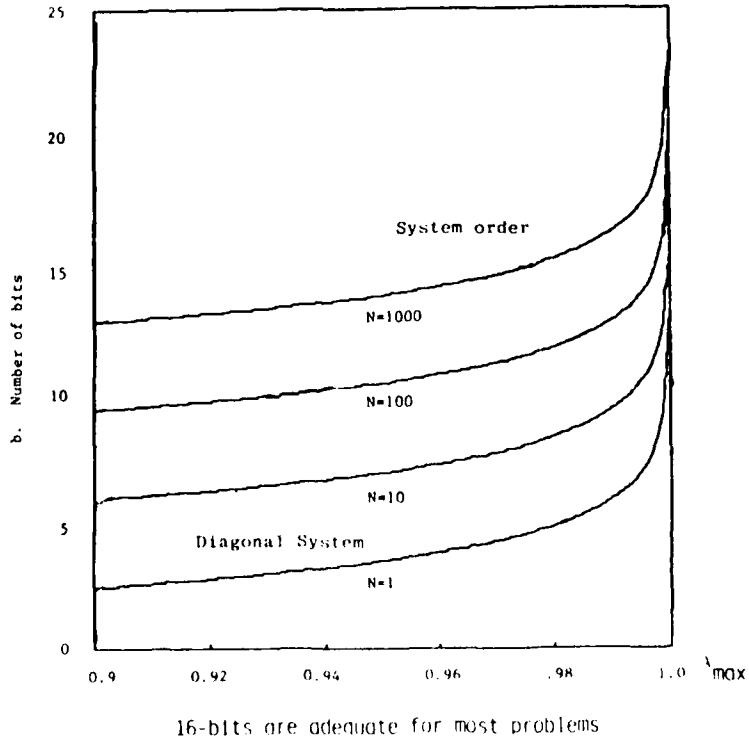

Figure 1-22 Minimum Number of Bits for Stable Control Computations

given digital flight control law. The magnitude of the maximum eigenvalue of F_{11} is the parameter which defines the margin of stability. The equation was evaluated for different values of λ_{max} and n. The results are shown in Figure 1-22. Note that the number of bits required for stability increases substantially as $\lambda_{max} \rightarrow 1$ and as n increases.

This formula represents an effective numerical test for rapidly determining the minimum number of bits required to implement a given digital flight control law. The magnitude of the maximum eigenvalues of F_{11} is the parameter which defines the margin of stability = $1 - \lambda_{max} = \Delta\lambda$. The equation was evaluated for different values of λ_{max} and n. The results are shown in Figure 1-22. Note that the number of bits required for stability increases substantially as $\lambda_{max} \rightarrow 1$ and as n increases. Because λ_{max} is directly related to the sampling rate $(1/\Delta\tau)$, Figure 1-22 indicates, therefore, that at high sampling rates, a large number of bits are needed to keep the computations stable. Since the improvement in stability is marginal beyond 16 bits, a 16 bit arithmetic processor is used.

Preliminary evaluation of the stability computations was made on a simple dynamic plant (4th order) to illustrate the technique. An F-15 digital longitudinal autopilot, used for flight tests, is shown in Table 1-XXI. Subsequent tests will be performed on CSDL #2 and the wheel closed-loop controller.

In the digital design a sampling rate of $1/\lambda$ = 100 Hz was selected. The sampling rate is about 50 times the Nyquist rate for the F-15. At such high sampling rate, the discrete implementation approaches the continuous design.

Note that all the eigenvalues of the closed-loop system are inside the unit circle. The minimum number of bits for the computations to remain stable in this F-15 aircraft example is also shown in Table 1-XXI.

Example: Digital Controller for F-15 Aircraft

- Digital Controller (100 Hz sampling rate)

$$\hat{x}_{k+1} = F_{11}\,\hat{x}_k + F_{12}\,y_k \qquad U_k = F_{21}\,\hat{x}_k$$

$$F_{11} = \begin{bmatrix} 0.9026 & -0.2986 & 0.0150 & -0.3143 \\ 0.0081 & 0.9945 & 0.0041 & -0.0026 \\ 0.0196 & -0.0422 & 0.9300 & -0.0480 \\ 0.0077 & -0.0012 & 0.0061 & 0.9990 \end{bmatrix}$$

- Eigenvalues of F_{11}

$$\lambda_1 = 0.9074,\ \lambda_2 = 0.9985,\ \lambda_{3,4} = 0.9601 \pm j0.0608$$

- Minimum Number of Bits for Stability

$$b = \left\lceil -(1 + \log_2((1-\underbrace{0.9985}_{\lambda_{max}})/4)) \right\rceil = 11 \text{ bits}$$

Table 1-XXI Emulation of Closed-Loop Control

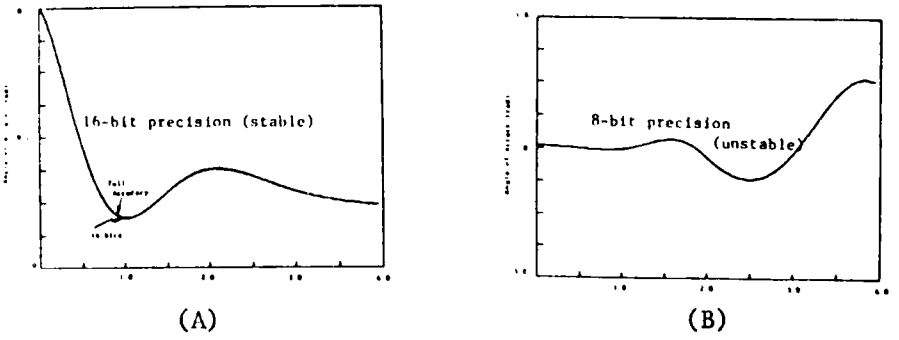

(A) (B)

Simulation results indicate that 16-bit precision is adequate for stable digital control computations.

Figure 1-23 Digital Controller Emulation: F-15 Angle of Attach Response

The closed loop dynamics of the F-15 aircraft were simulated with various levels of precision. The processor was emulated using 8-bit precision, 16-bit precision and 64-bit precision. Simulated values of the aircraft's angle of attach response are shown in Figure 1-23.

Figure 1-23A indicates that the control computations were essentially the same using 16-bit and 64-bit precision. Therefore, 16-bit precision was adequate for the control computations and F-15 aircraft remain stable.

However, Figure 1-23B indicates that if only 8-bits of precision are used, the F-15 will go unstable. Note that this result is consistent with the prediction that 11 bits are needed for stability.

Architecture of the Controller

The architecture of the processor is centered around a high-speed matrix-vector multiplier (see Figure 1-24). The control design matrix elements are stored in data memory and then downloaded into a high-speed RAM. The analog measurement data are converted to digital form by a high-speed, 12-bit, A/D converter. The results are stowed in a high-speed RAM along with the state estimates. The control law is then evaluated by multiplying the control-design matrix by the state estimates and measured data in RAM. A high-speed, 16-bit hardware multiplier/adder performs the matrix multiplications and additions required. All addresses for the RAMs and hardware multiplier/adders are generated by the firmware. The digital controls are then sent to a 12-bit D/A converter. The D/A converts the digital controls to analog signals which are stored in sample-and-hold circuitry. Once the controls have been updated, the controls are simultaneously sent to the actuators.

Requirements for Anti-Aliasing Filters

Digital controllers may require analog filters to eliminate unstable interaction between the controller and the unmodelled bending modes that sampling aliases into the controller frequency band. Also, such filters

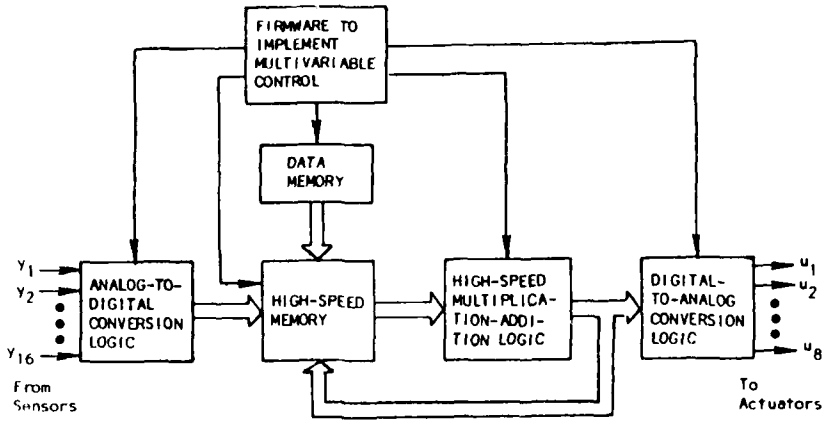

Figure 1-24 An Architecture for High-Speed Control

help reduce the noise aliased into the control band and the excitation of unmodelled resonances by harmonics in the reconstructed analog control signals.

So far, a simple example has demonstrated how an analog filter improves a rigid body controller's stability when sampling folds a single unmodelled bending mode whose damping ratio is 0.01. Both a classical and an optimal attitude controller were designed neglecting the effect of the bending response. These were exact discrete designs to eliminate the possibility of errors from discretizing a continuous control design. Figure 1-25 shows the block diagram of the total system.

Figure 1-26 charts the maximum possible controller bandwidth relative to the Nyquist frequency versus the bending-frequency to Nyquist-frequency ratio. Regions (1) through (5) all fold into region (0) like a fan. Line "a" indicates the bandwidth obtainable if no bending pole (i.e., pole corresponding to the bending mode) were present. The striped portions of the curves indicate that the attitude controller is unstable for higher bandwidths; unstriped portions indicate the highest obtainable bandwidth when the controller remained stable.

A cycle of z-plane bending pole movement from B to A and back is common to regions (0 and (1), (2) and (3), and (4) and (5). The bandwidth-limit curve exhibits a W shape in each case. At the arms of the W the pole is at B in the z-plane and the maximum bandwidth compares with the ideal limit 'a' because the large open-loop rigid body response near zero frequency dominates the folded bending response. At the center of the W the bending pole is at A, and the maximum bandwidth is again high because an open-loop phase shift of -360° at the bending resonance turns the resonant peak away from the point (-1,0) that determines stability in a Nyquist plot.

In summary, Figure 1-26 indicates that in this example an optimal controller bandwidth below 1/7th the bending frequency or 1/10th the Nyquist frequency will ensure stability. In contrast, a bandwidth less than 40 percent of the Nyquist frequency is safe for a classical design.

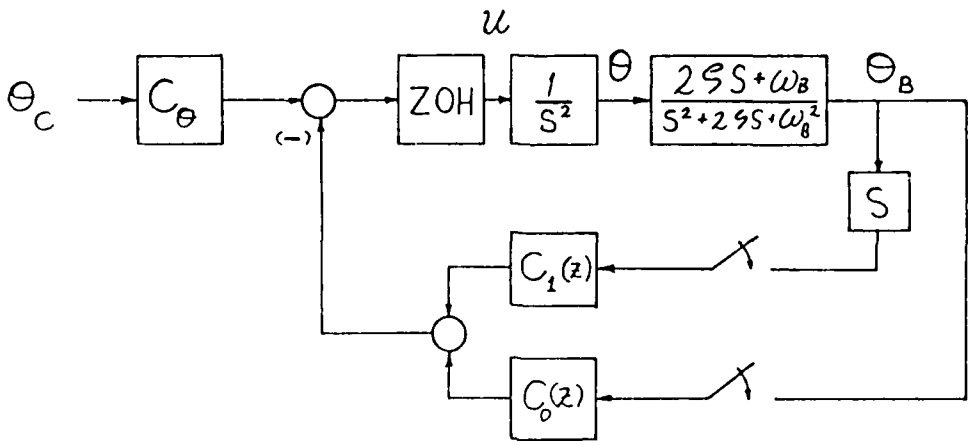

LEAD COMPENSATION: $C_1(Z) = 0. \; ; \; C_0(Z) = K \frac{Z + A}{Z + B}$

OPTIMAL DESIGN: $C_1(Z)$ MINIMIZES $\int_0^\infty (A\theta^2 + B\,u^2)\,dt$

Figure 1-25 Plant & Control Loop Schematic

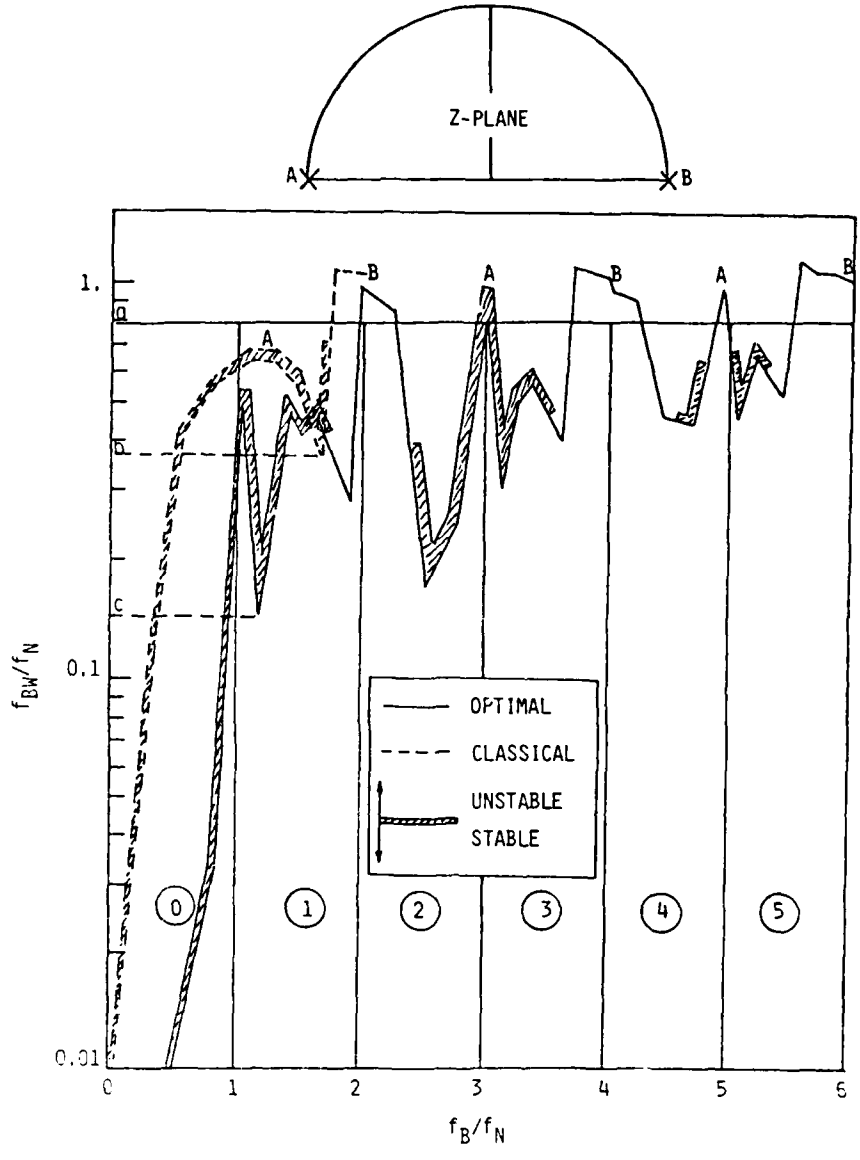

Figure 1-26 Maximum Bandwidth vs Bending Frequency

To improve the stability of the optimal design, a first-order filter is placed on the commanded torque (see Figure 1-27). Compensating the filter's phase lag in the control design allows a low filter break frequency, which maximizes the filter's attenuation of the unwanted bending response. Figure 1-28 shows that adding the filter increases the maximum controller bandwidth unless the bending pole is at the favorable z-plane locations A or B. In particular the lowest bandwidth limit in the folding region (1) increases from "c" to "b". The filter is most effective at high frequencies; thus it reduces the unstable region in (3) and eliminates the unstable regions in (4) and (5).

In short, with a filter the maximum optimal controller bandwidth to ensure stability increases from 13.5 to 36 percent of the Nyquist frequency, and the maximum Nyquist frequency for unconditional stability increases from 18 to 29 percent of the unmodelled bending frequency. Judging from frequency response such as shown in Figure 1-29, a Nyquist frequency below 25 percent of the bending frequency or a controller bandwidth below 33 percent of the Nyquist frequency will insure good response. Without a filter the corresponding values are 14 and 10 percent.

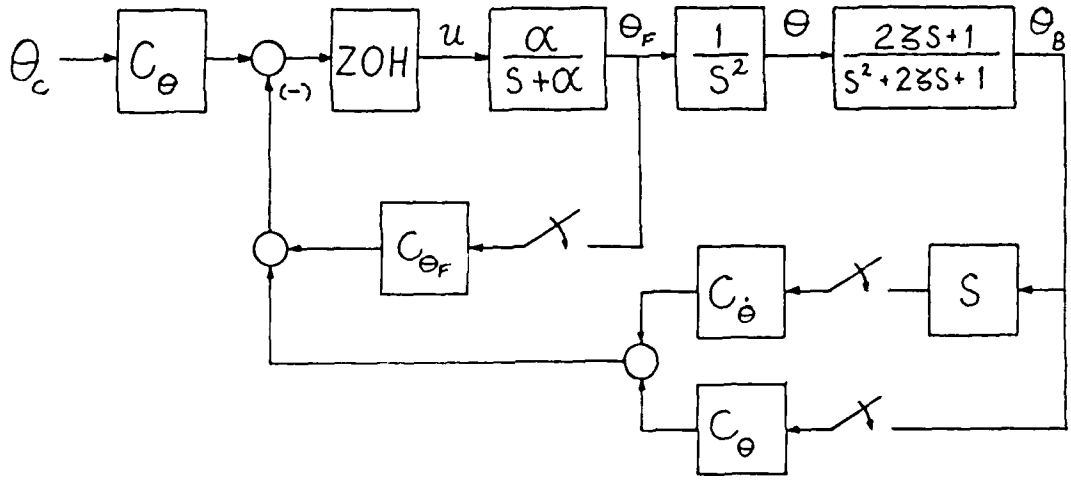

OPTIMAL DESIGN WITH PREFILTER: C_θ, $C_{\dot\theta}$, C_{θ_F} MINIMIZE $\int_0^\infty (A\theta^2 + B\,u^2)\,dt$

Figure 1-27 Optimal Design with Prefilter

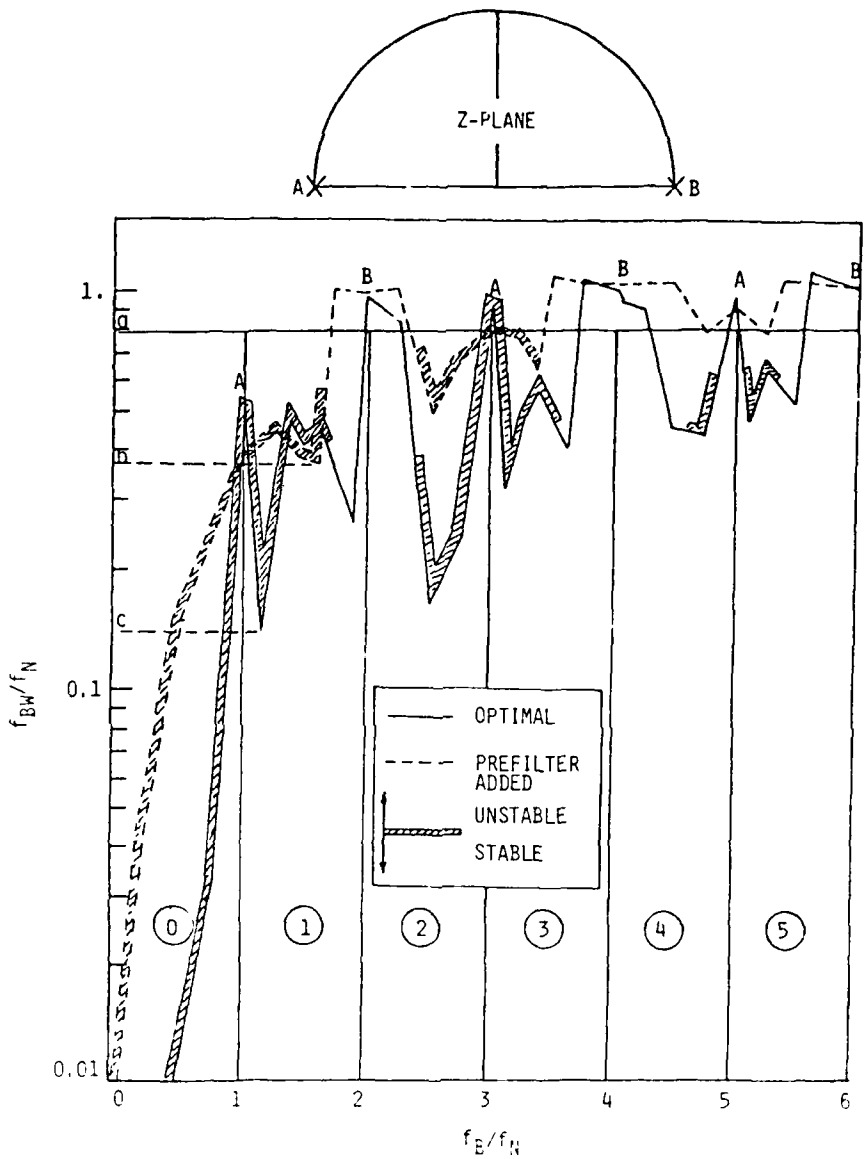

Figure 1-28 Maximum Bandwidth vs Bending Frequency For Optimal Controller with Filter

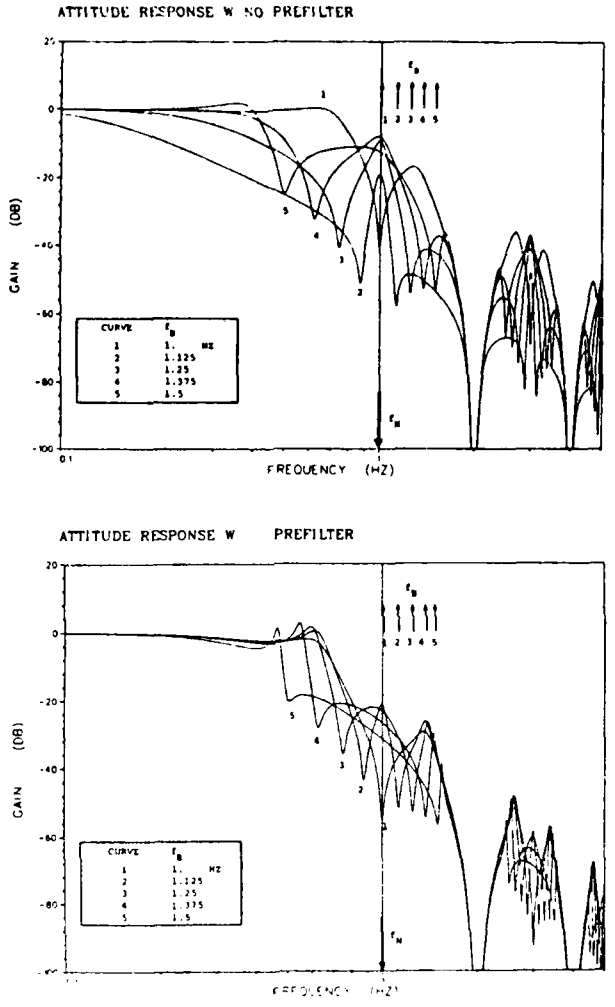

Figure 1-29 Closed-Loop Frequency Responses

2.0 EXPERIMENTAL VERIFICATION ON BRASSBOARD AND SYSTEM IDENTIFICATION TESTING (TASK 2.0)

2.1 LABORATORY EQUIPMENT UPDATE

The Dynamics and Control Laboratory has been physically relocated from Building 202 to Building 205 and several improvements and modifications have been made to the test equipment to reflect various experimental requirements.

2.1.1 Circular Plate Experiment

The test setup has been completely redesigned and is now totally mounted on a single 14 foot long Newport Research Optics Table as shown in Figure 2-1. At one end, the plate is hung by the suspension system shown in Figure 2-2, with the mounting bracket attached to a frame bolted on both sides of the table. To isolate the plate from acoustic vibrations and air motion, a wooden cabinet was built around the frame (but not touching it) and padded with sound absorbing material. A plexiglass cover closes this cabinent, allowing the view of the plate. To minimize air currents inside the cabinet, baffles have been installed on the back side and on the plexiglass cover as well.

At the other end of the optics table, is another frame supporting the optical measurement system. This system is shown schematically in Figure 2-3. It is mounted on a thick plate (weighing about 70 lbs.) resting on the two lateral pillars through vibration absorbing pads. There are also sheets of the same vibration absorbing material between the pillars and the optics table to which they are bolted. This new setup has reduced quite drastically the spurious noise induced by environmental vibrations, allowing the system to operate in the μrad range.

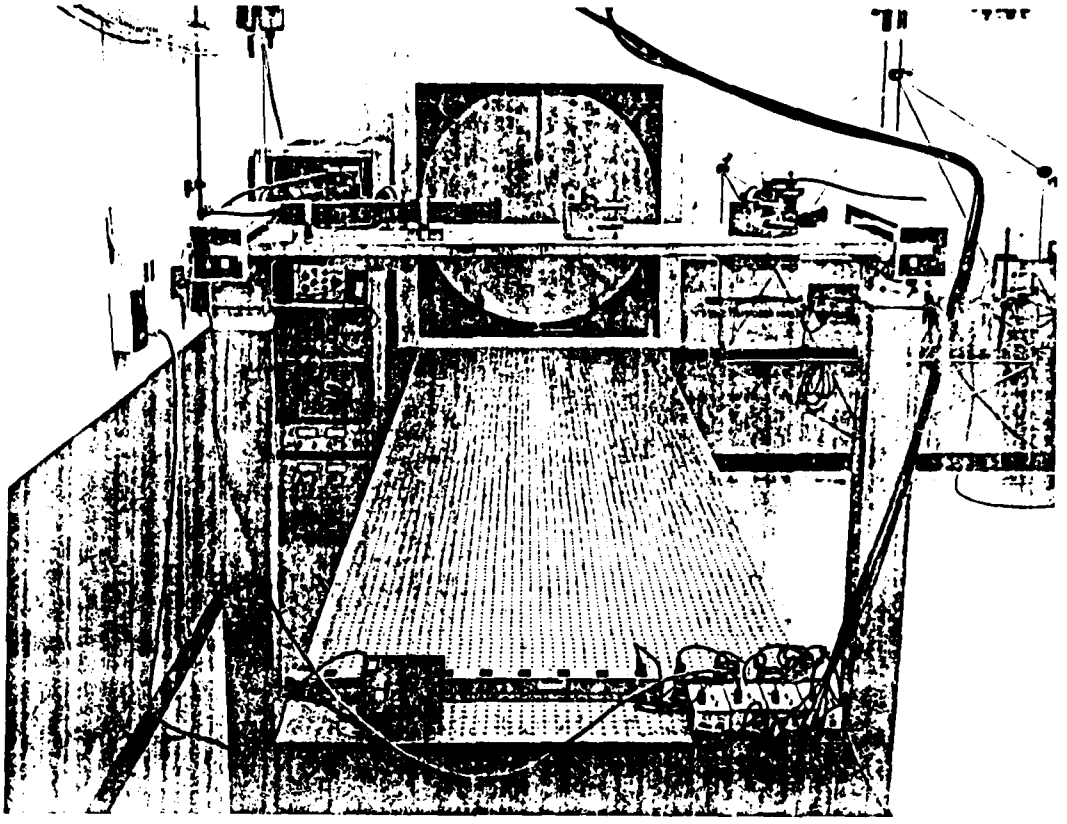

Figure 2-1 Plate Experiment Setup

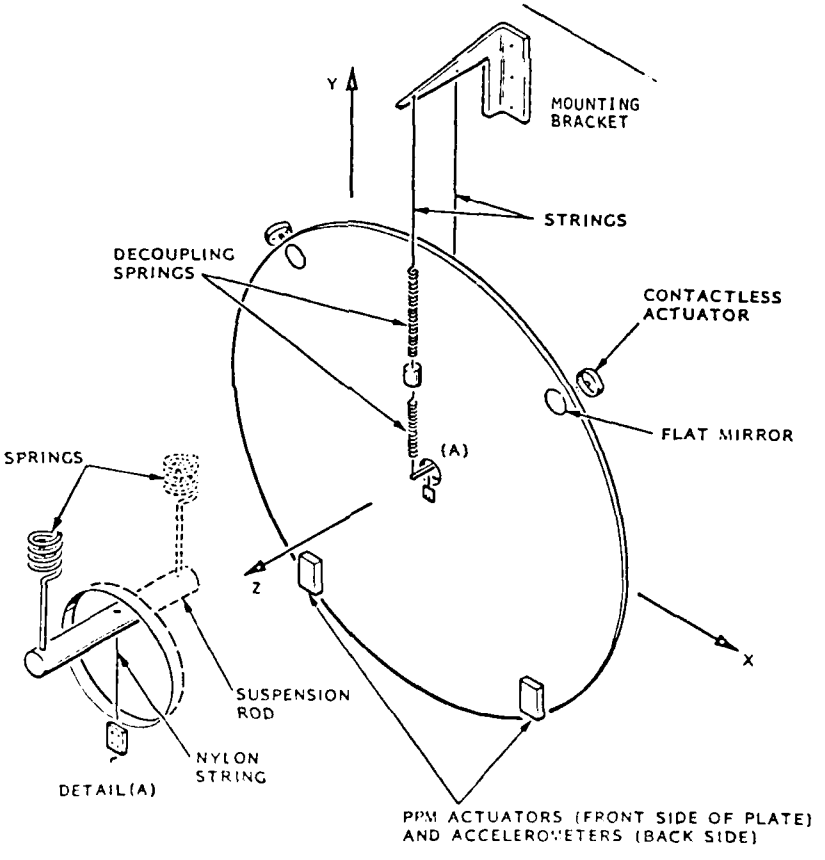

Figure 2-2 Plate Experiment

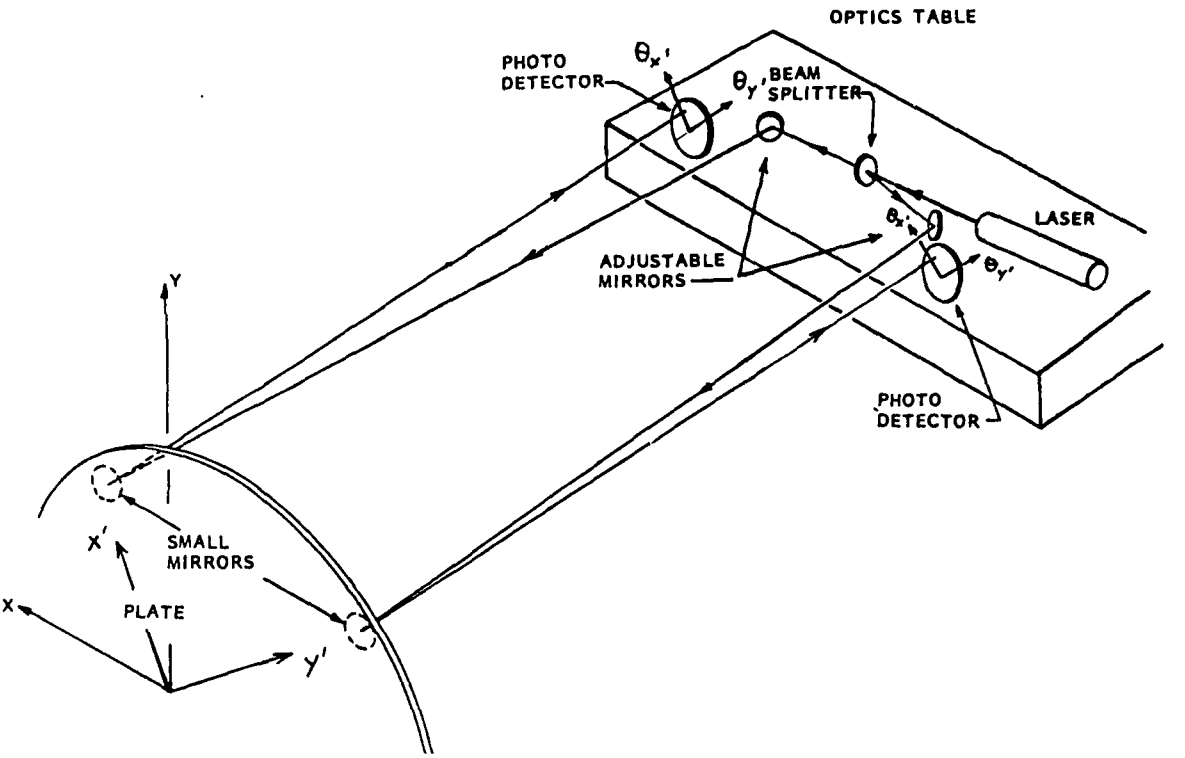

Figure 2-3 Optical Measurement System

SENSORS

①, ② : INERTIAL SENSING/ ACCELEROMETERS (1 D.O.F. Z-MEASUREMENT)

③, ④ : OPTICAL SENSING/MIRRORS
⑤, ⑥ : (2 D.O.F. $\theta_{x'}$, $\theta_{y'}$ ANGULAR MEASUREMENT

(x', y') ARE 45° W.R.T. (x, y)

⑦–⑩ : MICROPHASE OPTICAL SENSOR (Z DISPLACEMENT)

ACTUATORS

A_1, A_2 : PIVOTED PROOF-MASS

A_3, A_4, A_5 : CONTACTLESS ACTUATORS (5 MAY BE USED TO SIMULATE DISTURBANCES)

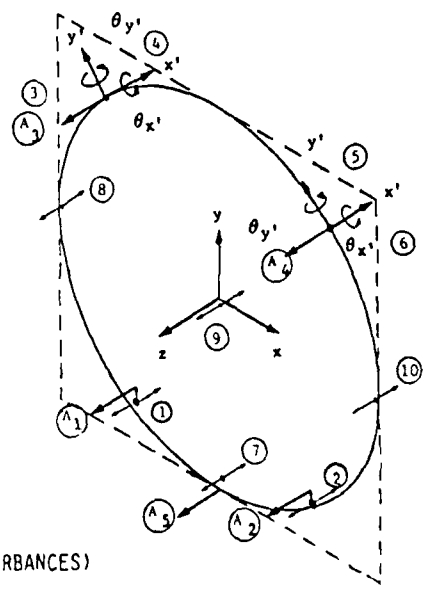

Figure 2-4 Plate Experiment Sensors and Actuators

The nature and location of the actuators and sensors used on the circular plate experiment are shown in Figure 2-4. The actuators are of two types:

1. Contactless Actuators - Magnetic forces are extended on a small magnet attached to the plate. This provides the necessary actuation for obsolute pointing.

2. Pivoted Proof-Mass Actuators (PPM) - Reaction forces are exerted by moving a small mass connected to the plate by an electrodynamic motor. Only AC forces can be produced this way.

Sensors are of the angular type (deflection of a light beam by a small mirror is sensed by a linear photo detector), or of the linear displacement type (measured via phase difference of the return light from a corner mirror using μ-phase detectors). In addition, accelerometers are used to measure vibrations along the Z axis.

2.1.2 Wheel Experiment

This test setup has also been installed in the laboratory. The bracket holding the wheel suspension system is mounted on a concrete wall. Four optical detectors have been installed on the wheel, six accelerometers and four Pivoted Proof Mass (PPM) Actuators. Figure 2-5 shows the general nomenclature used for this system of actuators and sensors. The PPMs driving electronic has been installed in a mobile bay and the general setup is shown in Figure 2-6.

For the open-loop characterization test, 15 measurement channels were connected to the 11-23 processor, comprising 8 optical channels, 6 accelerometers and a force measurement channel corresponding to an accelerometer mounted in lieu of the proof-mass on the PPM actuator chosen for exciting the structure.

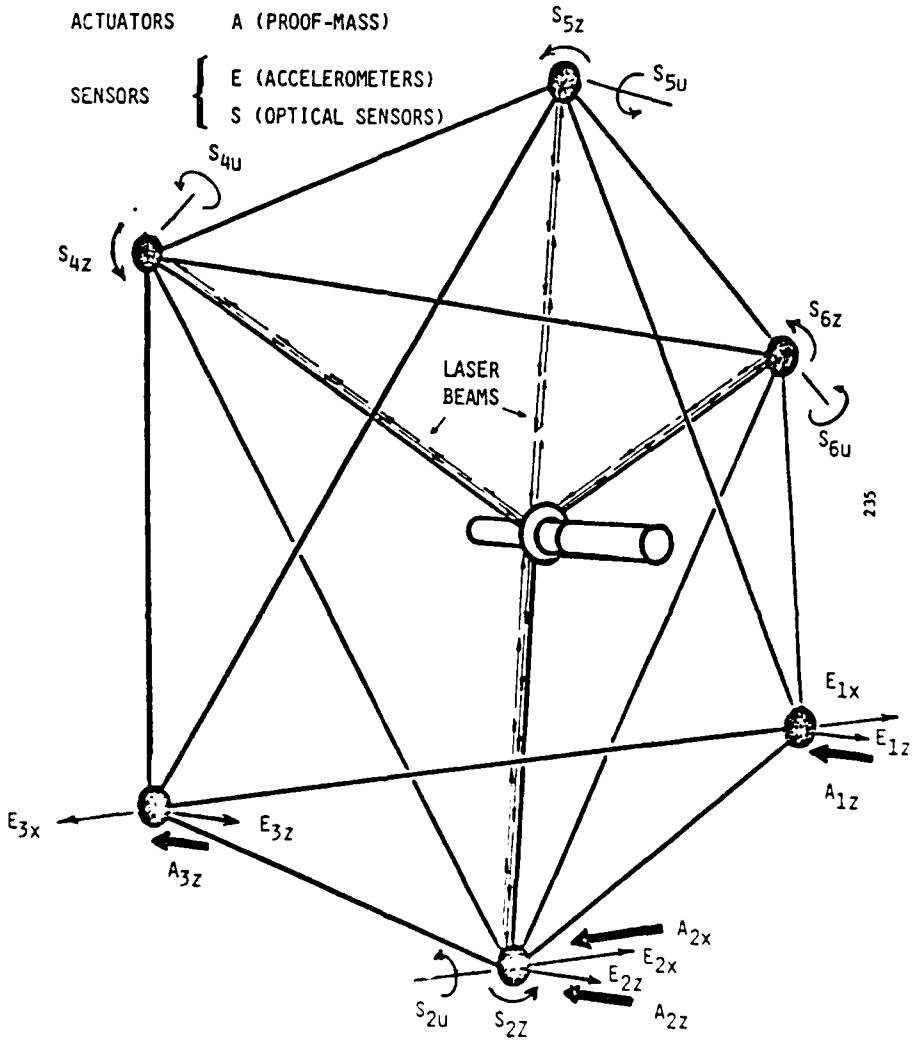

Figure 2-5 Wheel Actuators and Sensors

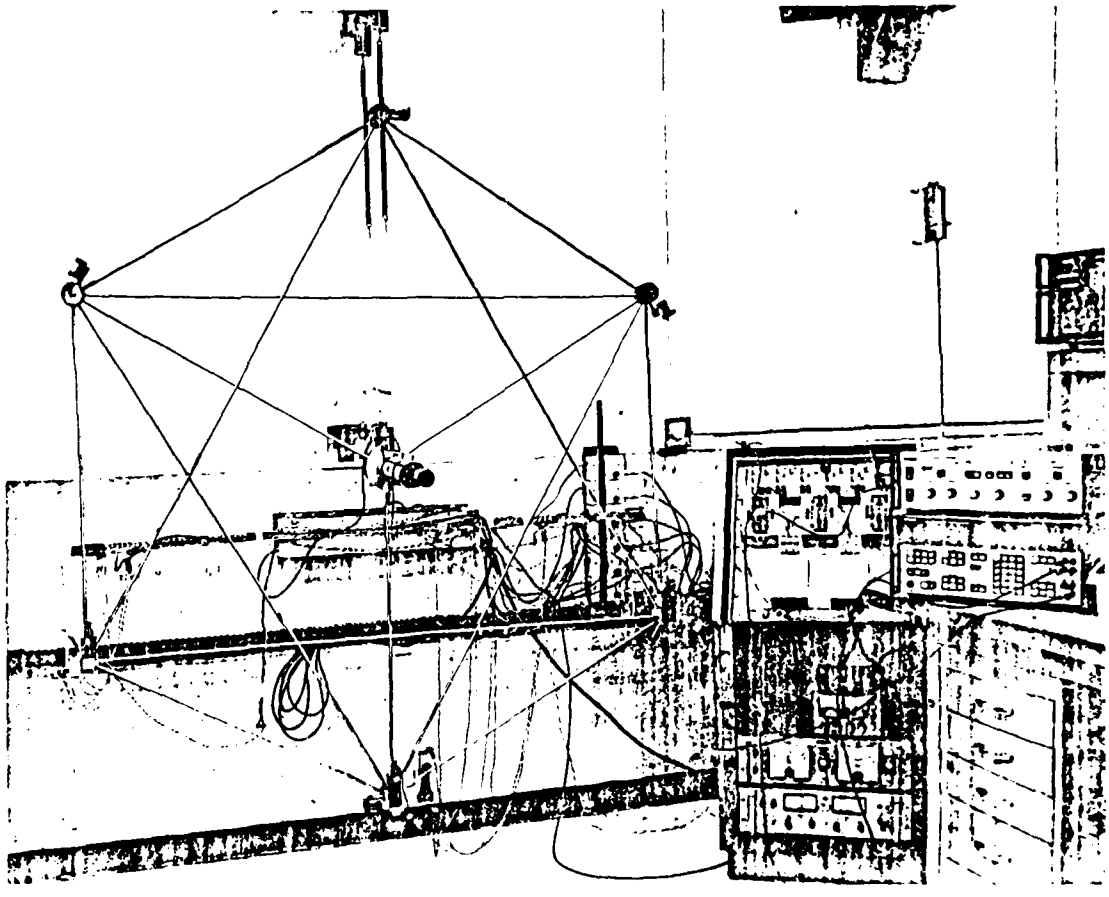

Figure 2-6 Wheel Experiment Setup

2.1.3 Digital System Status

The existing data processing/digital controller system has been given the added capability to communicate directly with large scale computers such as the Lockheed-based UNIVAC 11-23, the I.S.I. VAX computer, etc. This allows a direct transmission to the system to control gains generated by large scale Control Synthesis programs and also, the transmission from the system of time histories for off-line processing by large scale System Identification programs. The overall configuration of the digital system is shown in Figure 2-7.

This figure shows the interaction and interfaces between the various processors and the test structure. Control gains generated by control synthesis programs on the UNIVAC 1110 are transmitted directly to the STI/DEC 11-23 microprocessor system and stored in disk. These gains can then be loaded, when needed, in the Array Processor (AP) before starting control experiments. The AP has its own A/Ds and DACs and thus carries out the control of the specimen independently of the rest of the system. It can, however, be directed by the 11-23 to either start or stop controlling, or to acquire a time-slice of data for later examination by the 11-23 software. Also, the 11-23 can run concurrently dynamic characterizations of the specimen (either open or closed-loop) since it can acquire sensor data and send excitation signals via its own A/Ds and DACs.

The MAP300 Array Processor is now operating satisfactorily at 120 Hz sampling rate. Failures have been extremely rare since the beginning of the year and were very mild, i.e., the system could be restarted easily. An emulation of the array processor calculations was implemented on the UNIVAC 1110. Strings of data generated by the AP were then run and compared on the UNIVAC and satisfactory agreement was found.

Finally, new VAMP software was implemented, with "ZOOM" capability and "SWIFT" mode. ZOOM is a transformation which allows the data to be concentrated in a narrow frequency range, so that better resolution is obtained on a particular resonant mode. SWIFT (Sinewave Integration

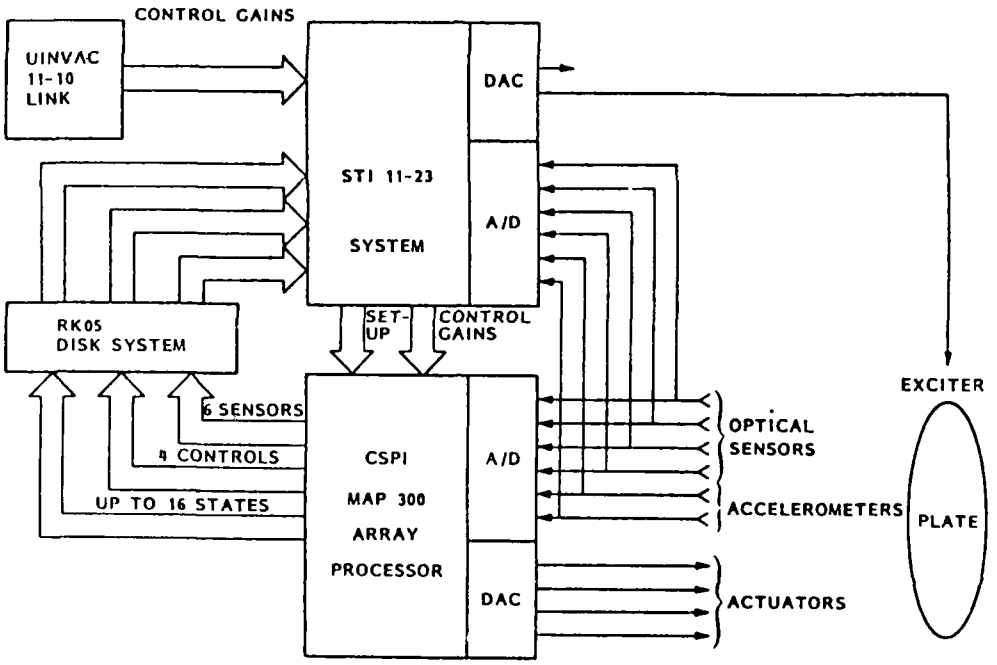

Figure 2-7 Overall System Configuration

Fourier Transform) is a technique for the high-accuracy determination of spectral properties of poorly damped structures. It uses sine sweeps with adjustable wait time and determines the Fourier components of the response.

2.2 EXPERIMENTAL PLAN

The experimental objectives of this study are summarized in Table 2-I. In order to reach these objectives, a test plan was established for each of the experiments. These test plans for the plate and the wheel experiment are described respectively in Table 2-II and 2-III.

OBJECTIVES	BRASSBOARD
o MODELING	WHEEL
o SYSTEM ID STUDIES	
(NEW VAMP, INSTRUMENTAL VARIABLES, MAXIMUM LIKELIHOOD)	PLATE, WHEEL
o SLATE ESTIMATION	PLATE, WHEEL
o HAC/CAL STUDIES	
(MODAL CONTROL, DISTURBENCE REJECTION, SPILLOVER)	PLATE
o μ-VIBRATIONS	PLATE

Table 2-I Experimental Objectives

Table 2-II is a matrix overview of the different types of controllers to be studied on the circular plate and the objectives of each of them. The actuators in use in each case are listed. The simplest controller, using only 2 contactless actuators (CEM) is essentially an attitude controller. Its main purpose is to check out the array processor algorithm and the calibrations so that confidence may be built up to study higher order controllers. This is an important and necessary step in this experiment.

EST #	PURPOSE	CONTROLLER TYPE	ACTUATORS NUMBER & TYPE	MODES CONTROLLED	DISTURBANCE TYPES	REMARKS
1	SYSTEM AND CALIBRATIONS CHECK OUT	CLASSICAL (P.I.D)	2 CEM	2 RIGID	1, 2	DIGITAL IMPLEMENTATION OF ANALOG STABILIZER; 2 OPTICAL SENSORS ONLY. TOTAL OF 4 STATES
2	FILTER ALGORITHM & ACCELEROMETERS CHECKOUT	HAC	2 CEM	3 RIGID	1, 2	4 OPTICAL SENSORS & 2 ACCELEROMETERS
3	EFFECTS OF LAC	HAC + LAC				TOTAL OF 6 STATES
4	DEMONSTRATION OF MODAL CONTROL & PPM USE	HAC + LAC	2 CEM 2 PPM	3 RIGID 2 BENDING	1, 2	REQUIRES 2 ADDITIONAL STATES FOR FILTER FREQUENCY SHAPING. TOTAL OF 13 STATES
5	DEMONSTRATION OF S.S. DISTURBANCE REJECTION EFFECTS OF DISTURBANCE VARIATION	HAC + LAC	2 CEM 2 PPM 1 CEM EXCITER	3 RIGID 2 BENDING	1, 2, 3	TOTAL OF 15 STATES
6	MULTIMODE CONTROL	HAC + LAC	2 CEM 2 PPM	3 RIGID 5 BENDING	1, 2	TOTAL OF 19 STATES
7	MICROPHASE OPTICS CHECK OUT	HAC/LAC	3 CEM	3 RIGID	1.2	1 μPHASE SENSOR FOR TRANSLATIONAL MODE
8	MICROPHASE OPTICS DEMONSTRATION FOR MULTIMODE CONTROL	HAC/LAC	2 CEM 2 PPM	3 RIGID 5 FLEXIBLE	1.2	18 STATES 8 SENSORS

DISTURBANCES: 1 ENVIRONMENTAL NOISE
2 STEP FUNCTION
3 SINUSOIDAL

Table 2-11 Circular Plate Test Matrix Control Experiments

TEST #	PURPOSE	EXCITER LOCATIONS	METHOD	RESULTS
1	OPEN-LOOP MODAL CHARACTERIZATION	AZ1	NEW VAMP (SLOW SWEEP)	FREQUENCIES, DAMPING TRANSFER FUNCTIONS
2		AX1		
3		AZ3		
4	MODAL CHARACTERIZATION WILL LAC	AZ3	NEW VAMP INST. VAR. & MAX. LIKELIHOOD	SAME
5	STATE ESTIMATION	AZ3	OPTIMAL FILTER	FIRST 8 BENDING MODES

Table 2-III Wheel Test Matrix

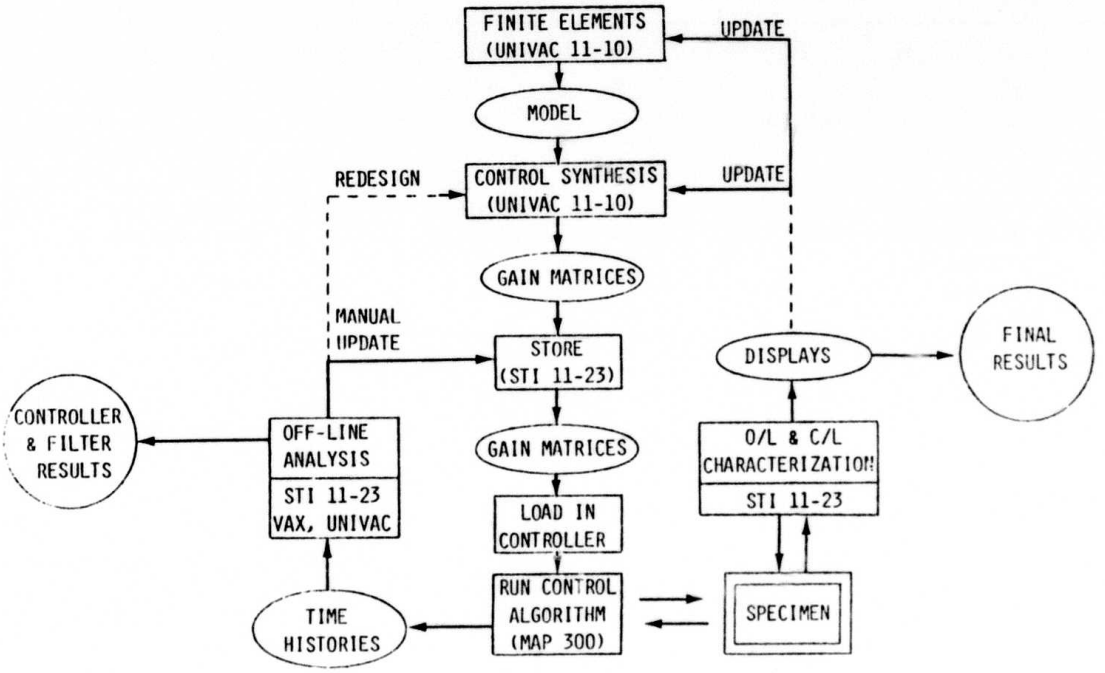

Figure 2-8 Control Experiment Procedure

For the last two controllers, disturbance will be generated via a third contactless actuator driven by either a pure sinewave (for steady-state disturbance rejection experiment) or a random excitation of given PSD.

The last two tests will use the newly developed μ-phase optical sensor. This device was tested open-loop in 1981 but has not been used yet in a closed-loop configuration.

Table 2-III gives a similar overview for the wheel experimental plan.

2.3 EXPERIMENTAL RESULTS

The various operations involved in the structural control experiments are shown in Figure 2-8. From the finite element analysis, a linear model is derived which is used as a basis for control synthesis programs. These programs generate a set of gain matrices which are stored in the 11-23 and may be manually updated if needed. The appropriate set is loaded in the array processor. Then the control algorithm is started and the AP controls the specimen and may acquire data. This data is stored on disk and can be analyzed off-line by the 11-23 or transmitted to a larger computer (VAX, UNIVAC 1110) for further processing. Also, while the AP is running, dynamic characterization may be carried out by the 11-23.

2.3.1 Plate Experiment

2.3.1.1 Digital Classical Attitude Controller

The first controller implemented on the Array Processor was the discrete version of the classical analog controller built in 1980 to stabilize the plate in rotation. It uses the signals from optical sensor #2 (i.e., sensors 5 and 6 of Figure 2-4 corresponding to the angular rotations θ_y, and θ_x, respectively) and two CEM. CEM actuators, each

actuator controlling separately its own axis (i.e., A_3 controls $\theta_{x'}$, A_4 controls $\theta_{y'}$). The digital mechanization of the control law is shown for one of the axes in Figure 2-9, along with continuous (analog) transfer function of the existing analog stabilizer. Figure 2-10 shows the angular rotations of the plate about its x' and y' axes when a step torque is applied about the x' axis and the digital loop is closed. The integral part of the controller makes the angle return to zero, exactly cancelling the disturbance (DC) torque. Figure 2-11 shows the closed-loop steady-state pointing error due to environmental noise. the RMS value is about 5 μrad.

2.3.1.2 Rigid Body Optimal Controller

An optimal controller was designed to control the 3 rigid body modes (2 rotations θ_x and θ_y, and 1 translation z). It uses the signals from the six sensors. The accelerometers measurements are integrated by an analog circuit to provide velocity measurements. The designed closed-loop poles were about 1 Hz for rotational modes with 60% damping, and .3 Hz in translation with 1% damping. The low damping in this mode resulted from the poor performance of the accelerometers at low frequency, making it difficult to correctly est-mate this mode. As a result some coupling is occurring with the rotational modes as can be seen in Figure 2-12.

This figure shows the output of the plate sensors when the rigid body controller is active and the plate subjected to a step input force at actuator #5 (CEM actuator at the bottom of the plate). The recovery time is about 1/3 sec. for the transverse axes ($\theta_{x'}$). The residual oscillation is due to the translational mode interaction. The state estimates can be used to reconstruct an estimate of the sensors signals, thus giving a check on the accuracy of those estimates and of the overall behavior of the filter. Figure 2-13 and 2-14 show respectively the time histories for $\theta_{y'}$ and V_z for both measured and estimated values.

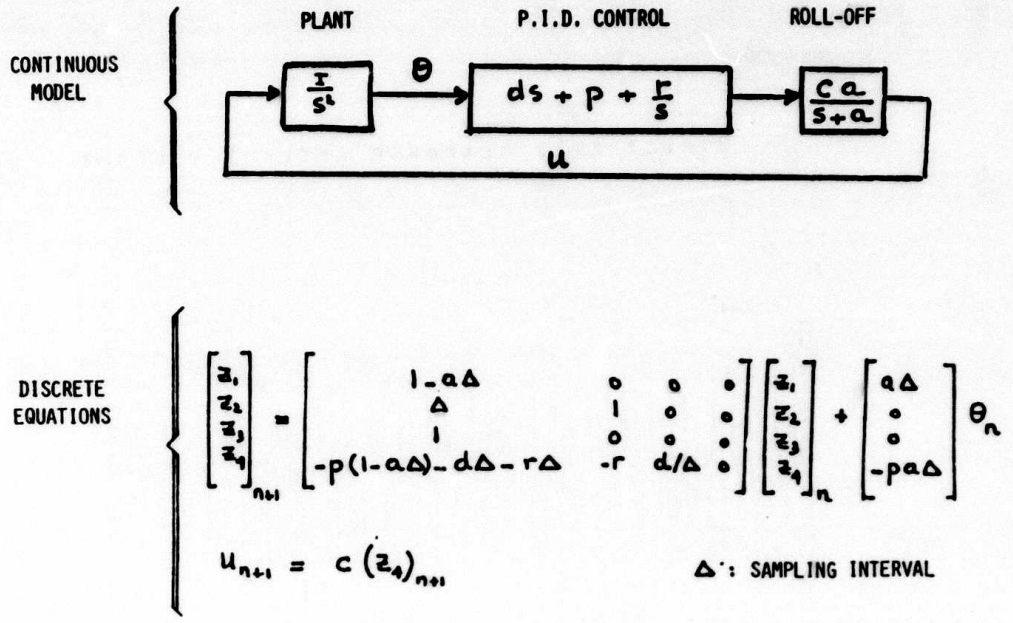

Figure 2-9 Plate Experiment: Classical Controller Discrete P.I.D. Controller with Roll-Off

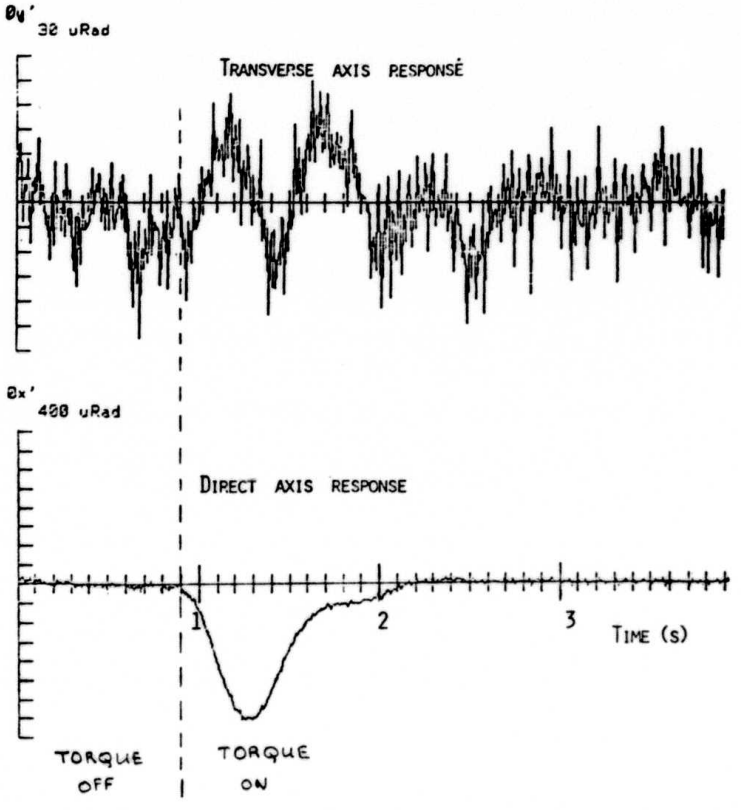

Figure 2-10 Circular Plate Response to Step Torque

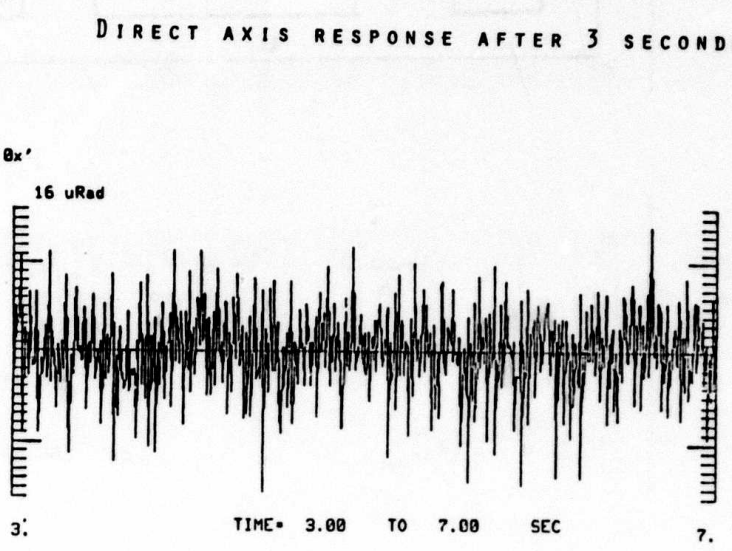

Figure 2-11 Circular Plate Response to Step Torque

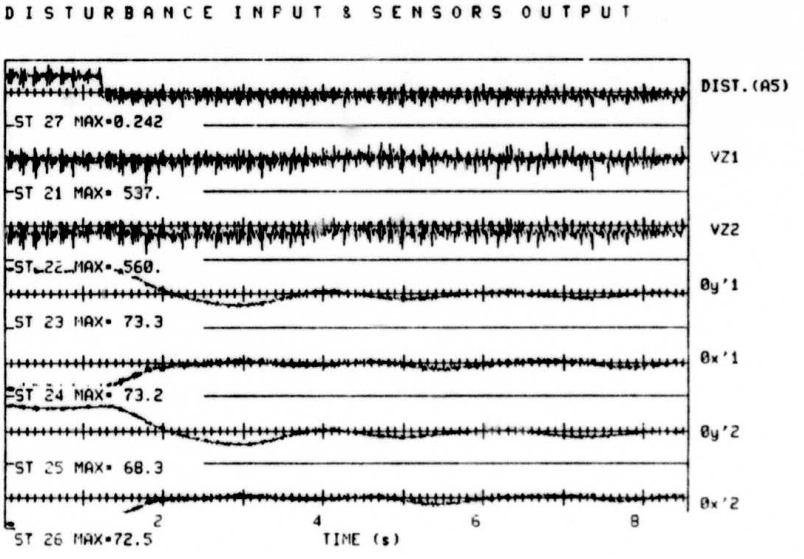

Figure 2-12 Circular Plate: Closed-Loop Test (HAC 3RB)

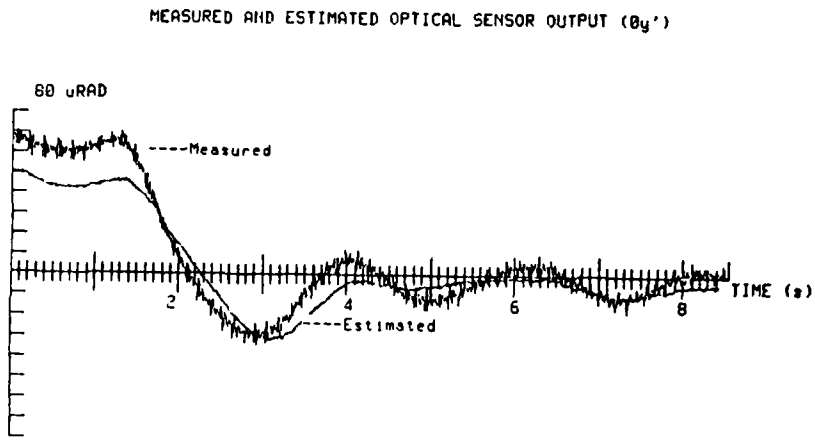

Figure 2-13 Circular Plate: Closed-Loop Test (HAC 3RB)

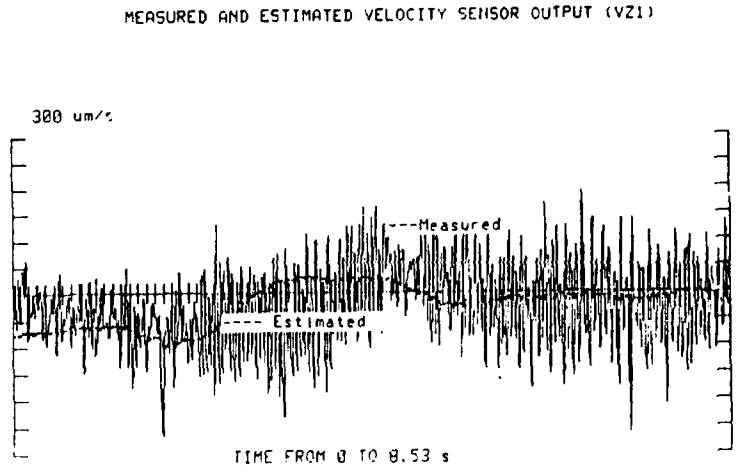

Figure 2-14 Circular Plate: Closed-Loop Test (HAC 3RB)

2.3.1.3 Modal Controller

The next controller studied included the 3 rigid body modes plus the first 2 flexible modes. Because of the low performance of the accelerometers at low frequency, the filter (state estimator) was modified to discard the low frequency information, but keep the relevant information around the modal frequencies. Controllability/observability problems have been encountered because the two flexible modes are very close in frequency and the system seems very sensitive to parameter errors. This matter is being investigated. A relatively low performance was however obtained with the loop closed on only the two CEM actuators. In this case about 9% damping was obtained in the highest mode, but only 1/2% in the other. An example of the closed-loop response is shown in Figure 2-15. The excitation was at the first mode frequency ($\sim$ 18 Hz). The second mode (poorly damped) was at about 19 Hz.

2.3.2 Wheel Experiment

2.3.2.1 Finite Element Model

Front and side views of the wheel finite element model are shown in Figure 2-16. The center hub consists of a laser tube with balance weights at one end. The corners of the wheel have adorned on it mirrors and Pivoted Proof Mass (PPM) actuator/accelerometers at selective places. The wheel itself consists of stainless steel tubes (10 mil thickness, 3/8" O.D.). A 3 dimensional view of the complete wheel model is shown in Figure 2-17. It consists of 636 degrees of freedom finite-element model. It weighs 36.4 lbs which exactly agrees with its measured weight. In Figure 2-18, the model frequencies and behavior patterns are listed and model mode numbers are shown for identification reference.

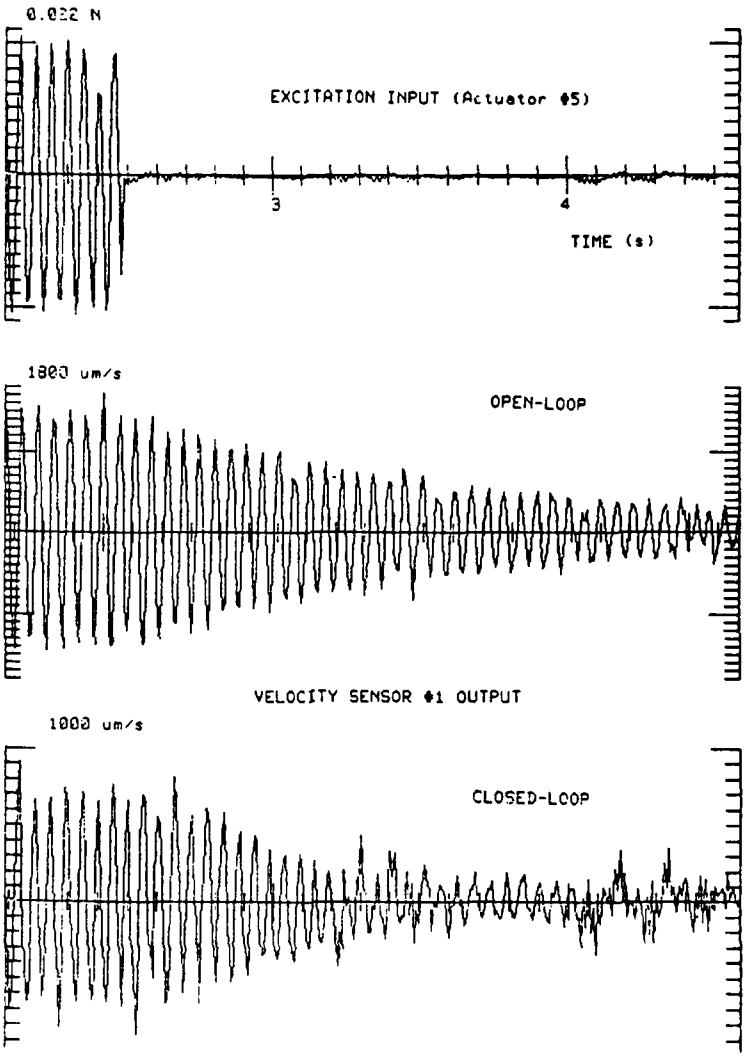

Figure 2-15 Circular Plate: Closed-Loop Test (3RB, 2F)

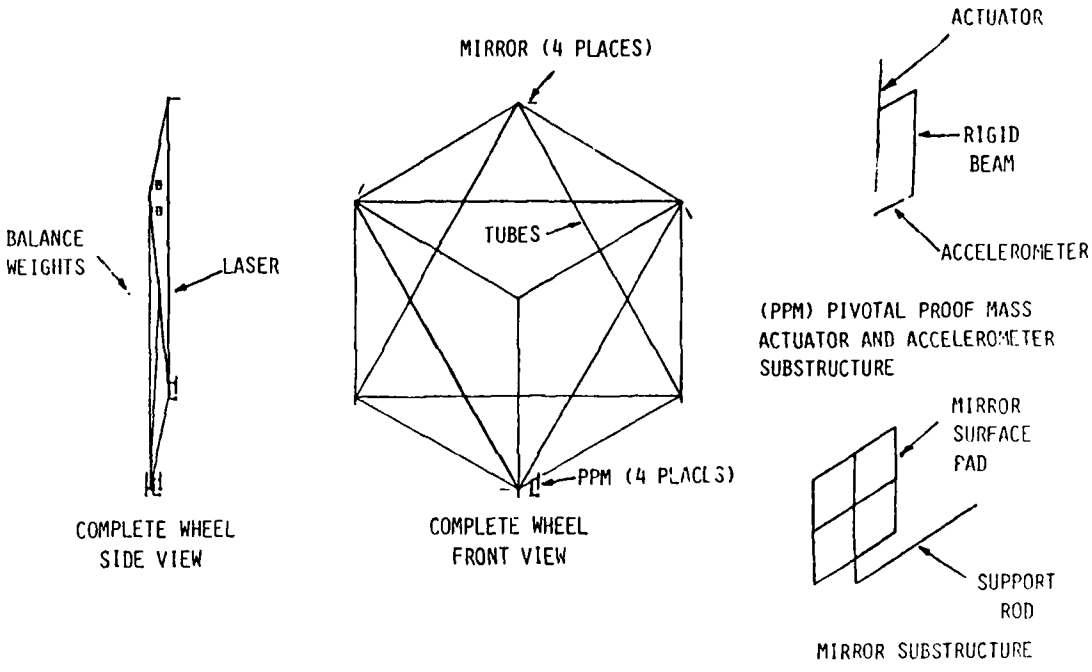

Figure 2-16 Components of the Wheel Finite Element Model

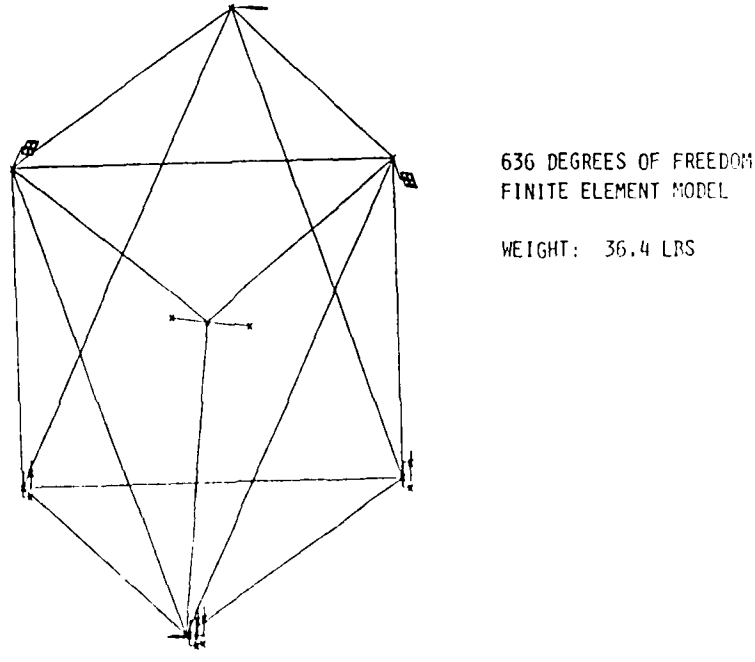

Figure 2-17 Complete Wheel Model

MODE #	FREQUENCY (HZ)	BEHAVIOR
1	3.63	CENTER HUB Y
2	3.64	CENTER HUB X
3	7.41	CENTER HUB Z
4	11.37	RODS (1-3) (5-1) BOW
5	13.49	ROD (2-4) BOWS
6	14.26	POINT 4 ROTATION
7	14.61	ROD (6-4) BOWS
8	14.67	ROD (3-5) BOWS
9	15.42	POINT 3 ROTATION
10	15.45	ROD (5-1) BOWS
11	15.60	POINT 5 ROTATION
12	15.78	ROD (2-4) BOWS
13	15.94	ROD (1-3) (6-4) BOWS
14	16.24	ROD (6-2) (2-4) BOWS
15	16.47	ROD (6-2) (5-3) (6-4) BOWS
16	19.87	ROD (6-2) (2-4) (6-4) BOWS
17	19.87	ROD (6-2) (2-4) (6-4) BOWS
18	20.90	
19	23.46	
20	24.11	EVERYTHING
21	28.78	
22	30.38	

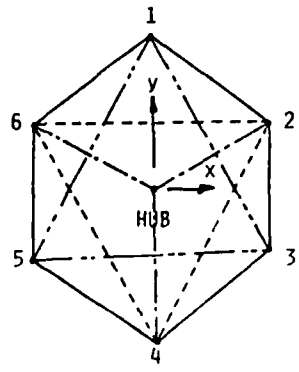

MODEL NODE NUMBERS
RELATING WHEEL LOCATIONS

MODEL WEIGHT: 34.6 LBS

Figure 2-18 Wheel Model Mode Identification

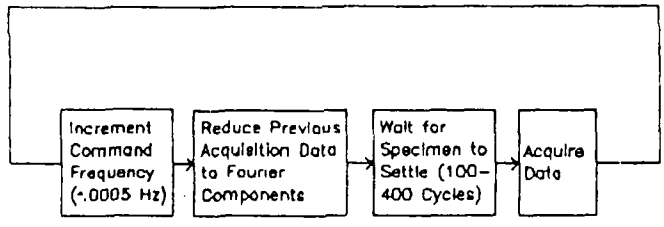

Figure 2-19 Sinewave Integration Fourier Transform SWIFT
(VAMP Implementation)

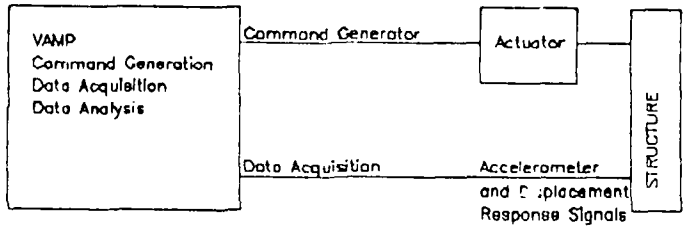

Figure 2-20 Structure Characterization Configuration

2.3.2.2 Identification Test

This test was run using the SWIFT mode of the VAMP program. The sequence of operations are shown in Figure 2-19 and the general setup in Figure 2-20. The actuator chosen to excite the structure was $A3_z$ (see Figure 2-5 for definition). The preliminary results of this test are given in Table 2-IV.

Mode	Frequency	Damping
1	3.48	
2	4.14	
3	7.27	.0012
4	10.83	.0029
5	12.12	.0020
6	15.23	.0016
7	15.52	.0015
8	15.75	.0015
9	16.90	.0014
10	18.12	.0013
11	18.58	.0013
12	19.36	.0012
13	20.63	.0012

Table 2-IV Experimental Characterization Results

2.3.2.3 Correlation of Test and Analysis

In order to do this comparison, it is necessary to identify the actual mode shapes. This was done by dwelling experimentally on each mode and directly observing the vibration patterns. The frequencies shown in Table 2-V are the only ones which could be directly compared since modes had the same shape (deformation pattern). The other frequencies (not compared) correspond to some combination of other mode shapes due to differences between analysis and test. These differences appear to be related to PPm substructures at points 3, 4 and 5.

TEST FREQUENCY (Hz)	ANALYSIS FREQUENCY (Hz)	BEHAVIOR
3.40	3.63	HUB Y
	3.64	HUB X
7.30	7.41	HUB Z
12.10	11.37	RODS (1-3) (5-1)
10.60	14.26	POINT 4 ROTATING
10.70	15.42	POINT 3 ROTATING
18.60	19.87	RODS (6-2) (2-4) (6-4) BOWS

Table 2-V Correlation of Test and Analysis

MODEL CHANGE	RESPONSE
• USING 4 SEGMENTED BEAMS INSTEAD OF 3 SEGMENTED BEAMS	INCREASE FREQUENCY .1 Hz FOR MODES ABOVE 10 Hz
• USING MEASURED Z OFFSETS INSTEAD OF THEORETICAL ONES	INCREASE FREQUENCY OF HUB Z MOTION FROM 7.5 TO 10.5 Hz
• ADD PPM SUBSTRUCTURE	2 NEW MODES IN (20 - 30) Hz RANGE AND (.2 to .5) Hz DECREASE IN MODES ABOVE 10 Hz.
• ZEROED HUB OFFSETS FROM CENTER TO RIM	.2 Hz DECREASE IN MODES BELOW 10 Hz (HUB MODES)
• ZEROED CORNER (1 - 6) OFFSETS	DECREASE (.1 - .2) Hz MODES BELOW 10 Hz DECREASE (.3 - .6) Hz MODES ABOVE 10 Hz

Table 2-VI Model Sensitivity

In an effort to get a better understanding of the discrepancies between model and actual structure, various model changes were performed to determine the sensitivity of the wheel frequency response. The results of this sensitivity study are listed in Table 2-VI indicating the significant influence of the PPM substructure model.

3.0 PROOF OF CONCEPT EXPERIMENT

3.1 INTRODUCTION

This section describes the plan for applying Active Control of Space Structures (ACOSS) controls technology to a scaled representation of a typical large aperture o-fset antenna spacecraft configuration in an extensive ground test for the primary purpose of validating the ACOSS technology. This test is devised to demonstrate the ability of the ACOSS technology to exert considerable control over and suppress the dynamic responses resulting from flexible body response of a realistic facsimile of a flexible spacecraft to typical orbital disturbances. The vehicle configuration, instrumentation and controls implementation are further designed to allow identification of hardware limitations and ultimate development of distributed sensor and actuator requirements.

3.2 OBJECTIVES OF THE PROGRAM

The specific objectives of the program are to:

- Experimentally demonstrate established ACOSS theory.
- Investigate hardware limitations and requirements.
- Investigate sensitivity of control approach to knowledge of the system model.
- Develop techniques for evaluating ACOSS control systems.

3.3 SCOPE OF THE TEST PLAN

This plan describes the activities required to accomplish the program objectives.

3.4 TEST SPECIMEN DEFINITION

The chosen configuration for the simulation is based on structural, schedule, cost and growth considerations. The result was a simulation of typical radial beam surface support structure dynamics/stiffness characteristics and a lightweight membrane surface. This structure appears as an RF reflector. The test specimen is presently designed, as shown in Figure 3-1, as a typical offset fed RF antenna system. To simulate as nearly as possible the free-free structural boundary conditions of the orbit environment, an air bearing suspension is employed. Control Moment Gyros (CMG) are used as the principle source of control torque, as is typical of orbiting systems which will result from this concept.

The CMG's planned for use in this test program are the Lockheed owned Bendix hardware. Since the bending modes to be controlled must be within the bandwidth of the CMG's, the design of the specimen is dependent on the characteristics of these CMG's; as a result, CMG characterization is a task included in the preliminary equipment test section. It is desired to keep primary bending frequencies between 1 and 10 Hz, and to insure that the corresponding modes are controllable by torques (CMG's) located in the vehicle bus (see Figure 3-1). Modes with bending frequencies between 10 and 20 Hz will be controlled by distributed actuators on Phases III and IV of the controls testing.

3.4.1 Design Procedure

- Determine preliminary beam sectional properties to ensure that the initial finite element model will have approximately the desired modal frequencies.
- Construct free-free finite element model of the specimen design approximate model parameter.
  - 250 modes
  - 1500 DOF's
  - 300 - 400 lbs

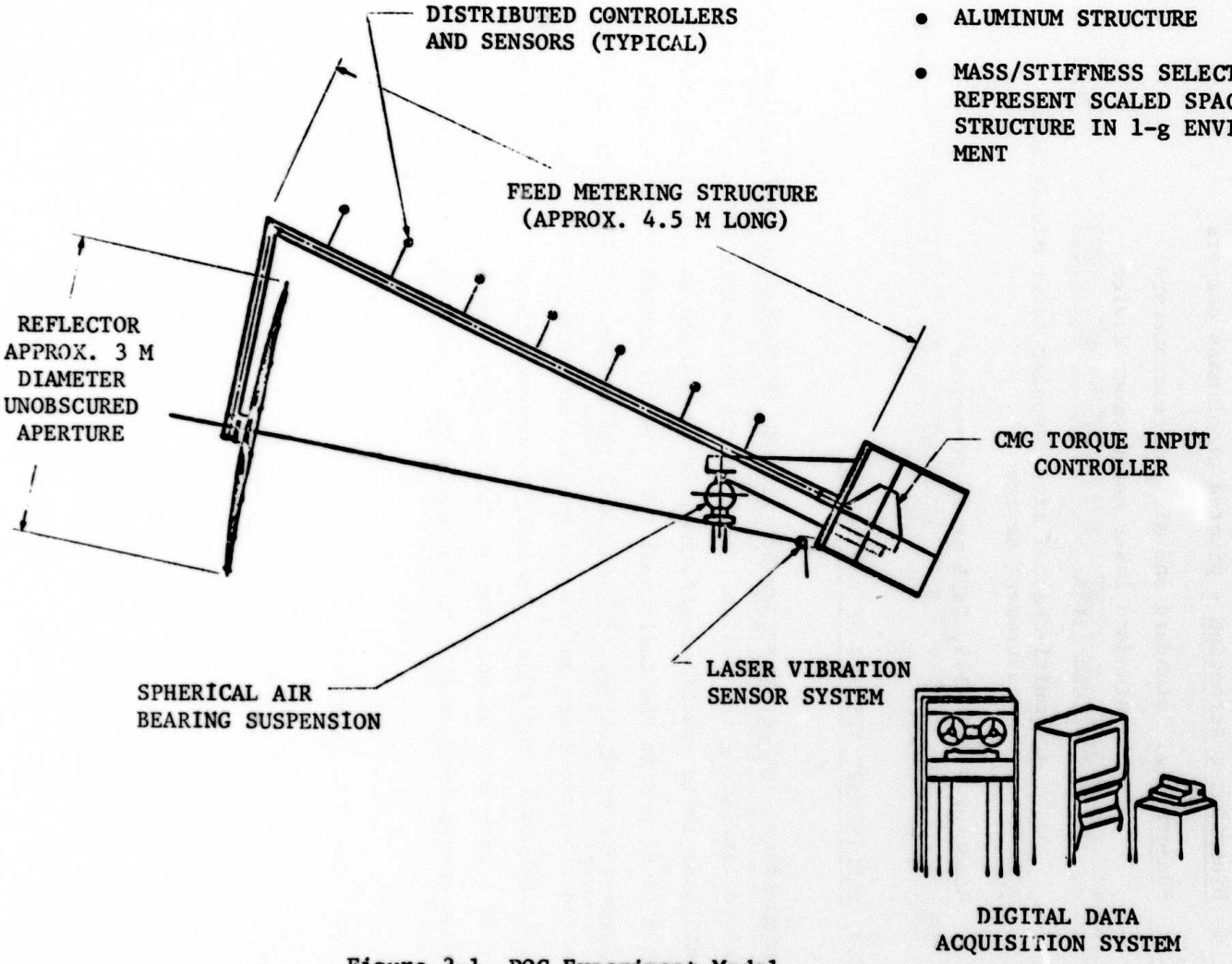

Figure 3-1 POC Experiment Model

Distributed Actuation - pivoted proof mass dampers

Sensors - a. standard and micro accelerometers

b. standard laser measurement device

c. rate gyros

d. multi-channel micro doppler laser displacement measurement device

Computer - PDP 1145, CSPI array processor

3.5 PRELIMINARY TESTING OF EQUIPMENT

As mentioned in Test Specimen Definition, CMG bandwidth data is required before finalizing the design. Also, since the Bendix CMG's are to be run well past their specified lifetime, it is desired to see if any anomalies have developed in the individual CMG's before assembling them into a single torquer package. In addition, the structural dynamics characterization requires tests on the air bearing to establish if a "pinned" structural boundary condition accurately represents the air bearing behavior, or if a more complex modeling of the boundary conditions at this crucial interface is necessary. The following outlines the plan for these tests.

3.5.1 CMG Characterization

The CMG tests to be performed will provide:

1. Gimbal Rate PSD for zero rate command input
2. Gimbal Rate Scale Factor
3. Torquer Cogging and Ripple
4. Tachometer Ripple
5. Open Loop Transfer Function
6. Nominal Wheel Speed

3.5.2 Air Bearing Characterization

The purpose of this test is to determine if the specimen-air bearing mounting will result in any new quasi-rigid body modes with frequencies below 30 Hz.

- Use instrumented hammer, accelerometers, and H-P transfer function analyzer to investigate unloaded air bearing for evidence of low frequency translational modes.
- If the above test is positive, increase complexity of test as necessary to adequately characterize modes in question.

3.6 PROOF OF CONCEPT TESTS

3.6.1 Test Preparation

Preliminary tasks to be performed before the start of testing are:

A. Preparation of the Flexible Vehicle Control Lab facility.

B. Mounting of CMG's in GAM configuration in specimen bus. Rate Gyros to be included on mount.

C. CMG distribution law to be implemented on PDP 1145.

D. Implement and test controls software. Implement and test data gathering software.

E. Mounting of specimen on air bearing in modal lab.

F. Preliminary installation and calibration of laser-grid sensing apparatus and accelerometers on specimen.

G. Interfacing of test with PDP 1145.

3.6.2 Phase I Test Specimen Modal Characterization

The Kalman filters used in many parts of the ACOSS control strategy require accurate models of that which is to be controlled. Because of this, any discrepancies between the final hardware setup and previously developed finite element models must be reconciled. The test proceeds as follows:

A. Design and implement simple control system to contain rigid body modes during test (this step later deleted).

B. Install accelerometers at locations as indicated by analytical modes.

C. Locate and support external actuators as necessary to perform modal test.

D. Install necessary instrumentation cabling and perform end to end checks.

E. Perform wide band sweeps to locate modes.

F. Perform narrow band sweeps for all modes of interest, 1 - 100 Hz range.

G. Process sweep data to obtain frequency, damping and mode shape date for each mode and any desired transfer function and influence coefficient data.

H. Perform additional tests as necessary to determine input-output relationships for control system actuator and sensor systems.

I. Refine finite element modal to concur with test results.

3.6.3 Phase II Test - Central Actuator Controls Experiment

During this phase, tests are run on control systems designed to use the central actuator package to greatly reduce the settling time of the LOS when provoked by transient disturbances.

The control systems to be tested in this phase are designed to return the LOS rapidly to its nominal direction after it has been deflected by some external disturbance. The disturbance can disrupt the LOS pointing either by changing the orientation of the entire test specimen, by changing the relative orientation of mirror and laser by bending the specimen, or by some combination of both. The control systems use only the central actuator package (CMGs) located in the ES of the specimen to control the LOS. In this early test stage, only the part of the LOS with frequency components at or below 10 Hz is controlled; that is, the controller will have an effective bandwidth of 10 Hz.

Two design approaches for the control systems are being considered. The first introduces, by active control, significant damping in all bending modes under 10 Hz, which causes them to settle down quickly after an excitation. When the rigid-body modes are controlled as well, the LOS settles down quickly itself. The other approach is to cause that particular combination of sub-10 Hz modes constituting the LOS to settle quickly. This approach differs from the first in that damping is not necessarily induced in any of the modes separately. Rather it causes them to respond together in such a way that the LOS settles down quickly after a disturbance.

Both design approaches are implemented in the same manner. They both use a Kalman filter to estimate model amplitudes and rates (including those of the rigid body), which are then fed back to the control actuator. The feedback of the estimates to the control actuator distinguishes the two approaches from each other; they both use the same estimator to obtain the modal amplitudes and rates. In this task, since only the behavior of the LOS in the frequency range below 10 Hz is to be controlled, only the first six bending modes of the test specimen are estimated and fed back.

A schematic of the POC test specimen equipped for Phase I tests was shown previously in Figure 3-1. The instruments used to provide inputs to the control system Kalman filter are also used to acquire evaluation

data during tests. Ten accelerometers are located on the ES, mast and antenna dish of the specimen; a three-axis rate gyro package is mounted on the CMG package in the ES; and a laser attitude determination system (not shown) is attached to simulate and measure the LOS orientation and to measure rotation of the ES about the LOS axis.

Before either type of control system is tested, the Kalman filter segment of the controller must be checked out. To accomplish this, the control gains are set to zero so that there is no control response and the specimen is subjected to a modal test as described in the Progress section. The modal test is conducted using a single electromechanical shaker whose frequency and point of application are varied to ensure excitation of all modes. Test data are obtained from the accelerometers, rate gyros, and laser attitude determination system and stored for post-test evaluation. The filter is then adjusted for proper response time and separation within the estimated states. When the Kalman filter is working properly, the control loop is closed and another test is run.

With the control system that seeks to impart damping to the individual bending modes below 10 Hz, this test is again a modal test, but it is performed this time with the control system in place and operating. For this control system, proof of success comes from frequency domain analysis of test data to show whether or not target damping values are attained for the closed-loop system. Transfer functions from the shaker input to the various outputs are constructed from the test data, and the modal peaks are examined to determine frequency damping for each mode in the controlled system.

For the other type of control system, a similar frequency domain analysis reveals the efficacy of the control system, but in this case the relative phases of the various modes must be taken into account so that the intermode cancellation can be detected. Also, in the time domain, a simple time history of the LOS response to a step input perhaps best reveals the performance of this system.

Preliminary goals for this test phase are to establish a control system that causes the sub-10 Hz component of the LOS motion to diminish by a factor of 1/e within 0.5 s. This can be accomplished by imposing 20 percent damping in the 10 Hz modes. For lower frequency modes, the frequency must be actively increased and significant damping must be imposed to meet the 0.5-s settling time goal.

A settling time goal of 0.5-s is quite conservative, and a 0.1-s settling time should be possible. However, 0.5-s is sufficiently quick to allow transition to Phase 2 tests.

3.6.4 Phase II Test - Distributed Controls Experiment, Transient Disturbance Rejection

During this phase, the Phase I setup will be augmented by up to 10 small force actuators distributed about the test specimen, with the goal to extend the control system bandwidth to 20 Hz.

The control systems to be tested in this phase will augment those verified in Phase II. The intent is to add a number of the small PPM actuators. With these additional actuators, the bending modes between 10 and 20 Hz can be controlled, and their disruption to the LOS can be reduced to the desired 0.5-s settling time.

That these additional modes are to be controlled with distributed actuation rather than with the centrally located CMGs is not because of the bandwidth of the CMGs; in fact, their response curve is flat out to 100 Hz. Distributed actuation is to be used because, even though the CMGs are powerful (each can exert up to 100 ft-lb), the leverage made possible by placing an actuator to optimally control one or two modes can easily offset the power advantage. For bending modes between 10 and 20 Hz, the forces necessary to actively impose 10 percent damping by exerting forces or torques from the CMG cluster can easily exceed the capabilities of the CMGs,

whereas a few proof-mass actuators, with a force capability of no more than 1 or 2 lb, can accomplish the desired damping if strategically located.

Aagain, the control system design can take either of two approaches; to independently damp all modes so that the LOS settles quickly or to control the bending modes to advantage so that the LOS settles within 0.5-s.

The test procedure is the same as that for Phase II.

3.6.5 Phase IV Tests - Distributed Controls Experiment, Steady State Disturbance Rejection

During this phase, tests are run on a control system designed to use distributed actuators as well as the central CMG cluster to diminish the effect of a steady state onboard disturbance on the LOS.

The control systems tested in this phase used the distributed actuator configuration assembled in the previous phase to significantly reduce the effect on LOS of constant disturbances with known frequency characreristics. These control systems superficially resemble those assembled for Phase III tests in that a Kalman filter is used to estimate modal activity and to feed back the modal estimates.

For this phase, the filter is augmented with new states to create the modern control analog of classical control "notching". This notching causes the control system to concentrate effort within a specified frequency band, that of constant disturbance, so that no energy is wasted outside that band. Since the disturbance is constant, damping and settling time are not goals of the control design. Rather than shift the eigenvalues of the controlled system farther to the left of the imaginary axis, these control systems work by modifying the mode shapes. The result is that, even when all modes are active (being driven by the constant disturbance), the mode

shapes are "dented" by the control system in such a way that the response of the LOS to the disturbance is greatly reduced. These control systems are designed to modify the bending mode shapes rather than to change their frequency domain behavior, as do the control systems used in Phase I and II.

In this phase, two disturbance sources simulated by a small electromechanical shaker are mounted on the test specimen, one on the antenna dish and one in the ES. They are driven simultaneously, but at different fixed frequencies. Their performance is evaluated by comparing the steady state response of the LOS (measured directly) in the controlled case to that for the uncontrolled case.

3.6.6 Phase V Tests

The testing in this phase of the experiment is designed to show the effect of several slewing techniques on the lower frequency bending modes. In particular, to demonstrate the ability of certain slewing methods to leave bending modes quiescent at the end of the maneuver.

The maneuver to be used to compare the various techniques is a 10° combination yaw-pitch slew to be executed in 10 s. This maneuver will excite all of the sub-20 Hz bending modes. It must be followed within 5 s by a return maneuver to avoid saturating the CMGs by requiring them to hold the POC specimen askew to gravity. The present CMGs are not adequate for performing any of these maneuvers, although their torque capacity (100 ft-lbs) is more than enough, their 5 ft-lb-sec momentum capability is at least an order of magnitude to small to carry out the requisite maneuver.

To perform these tests, a set of reaction wheels currently here at Lockheed must be modified to CMGs with more balanced specifications of 50 ft-lb torque capability while maintaining 50 ft-lb-sec of momentum.

The three slewing techniques to be used are:

1. Square Wave Slew - excites all the modes

2. Sine-Versine Slew - leaves one mode unexcited after maneuver

3. Optimal Slew - leaves all modes unexcited after the maneuver (but uses more power to do it)

Further we will show a method of closing a loop on the optimal slew in order to avoid parameter sensitivity.

3.6.7 Phase VI Test - Dynamic Figure Control

In this phase, the control systems of phases two and three are extended to control the 20 to 30 Hz bending modes of the antenna dish.

Ten small (1/2 lb) PPMs will be located symmetrically about the antenna dish. Displacement sensing with accuracy in the range of 10^{-4} inches will be provided by the micro-phase laser sensor developed earlier on the ACOSS contract. Initially, the control systems will be extended to provide active damping of the dish modes. However, by substituting small displacement actuators for the PPMs, this phase of the experiment could be expanded to demonstrate figure control of the antenna dish.

addresses	number of copies
R. Carman RADC/OCSE	5
RADC/TSLD GRIFFISS AFB NY 13441	1
RADC/DAP GRIFFISS AFB NY 13441	2
ADMINISTRATOR DEF TECH INF CTR ATTN: DTIC-DDA CAMERON STA BG 5 ALEXANDRIA VA 22314	12
Lockheed Missiles & Space Co. Space Systems Division PO Box 504 Sunnyvale, CA 94086	5
Charles Stark Draper Lab Dr. Keto Soosaar 555 Technology Square M.S. -95 Cambridge, MA 02139	1
Charles Stark Draper Lab J. G. Lin 555 Technology Square Cambridge, MA 02139	1
Charles Stark Draper Lab Attn: Mr. R. Strunce 555 Technology Square M.S. -60 Cambridge, MA 02139	1

Charles Stark Draper Lab
Attn: Dr. Daniel R. Hegg
555 Technology Square
M. S. -60
Cambridge, MA 02139 — 1

ARPA/MIS
1400 Wilson Blvd
Arlington, VA 22209 — 1

ARPA/STO
Attn: Lt Col A. Herzberg
1400 Wilson Blvd
Arlington, VA 22209 — 1

ARPA/STO
Attn: Maj E. Dietz
1400 Wilson Blvd
Arlington, VA 22209 — 1

Riverside Research Institute
Ms S. E. Bickerstaff
Attn. Mr. A. DeVilliers
1701 N. Ft. Myer Drive Suite 711
Arlington, VA 22209 — 3

Riverside Research
Attn: HALO Library, Mr. Bob Passut
1701 N.Ft. Myer Drive
Arlington, VA 22209 — 1

Itek Corp
Optical Systems Division
10 Maguire Rd.
Lexington, MA 02173 — 1

Perkin Elmer Corp
Attn: Mr. H. Levenstein
Electro Optical Division
Main Avenue
Norwalk, CT 06856 — 1

Hughes Aircraft Company
Attn: Mr. George Speak
M.S. B_156
Culver City, CA 09230 1

Hughes Aircraft Company
Attn: Mr. Ken Beale
Centinela Teale Sts
Culver City, CA 90230 1

Air Force Flight Dynamics Lab
Attn+ Dr. Lynn Rogers
Wright Patterson AFB, OH 45433 1

AFWL/FIBG
Attn: Mr. Jerome Pearson
Wright Patterson AFB, OH 45433 1

Air Force Wright Aero Lab. FIEE
Attn: Capt Paul Wren
Wright Patterson AFB, OH 45433 1

Air Force Institute of Technology
Attn: Prof. R. Calico/ENY
Wright Patterson AFB, OH 45433 1

Aerospace Corp.
Attn: Dr. G.T. Tseng
2350 E. El Segundo Blvd
El Segundo, CA 90245 2

Aerospace Corp.
Attn: Mr. J. Mosich
2350 E. El Segundo Blvd
El Segundo, CA 90245 1

Aerospace Corp/Bldg 125/1054 — 1
Attn: Mr. Steve Burrin
Advanced Systems Tech Div.
2400 E El Segundo Blvd
El Segundo, CA 90245

SD/SD/YLVS — 1
Attn: Mr. Lawrence Weeks
P.O. Box 92960
Worldway Postal Center
Los Angeles CA 90009

SD/YCD — 1
Attn: YCPT/Capt Gajewski
P.O. Box 92960
Worldway Postal Center
Los Angelel, CA 90009

Grumman Aerospace Corp — 1
Attn: Dr. A. Mendelson
South Oyster Bay Road
Bethpage, NY 11714

OUSDR&E/DS — 1
Attn. Mr. A. Bertapelli
Room 3D136
Pentagon, Washington, DC 20301

Jet Propulsion Laboratory — 2
Dr. S. Szermay
4800 Oak Grove Drive
Pasadena, CA 91103

MIT/Lincoln Laboratory — 1
Attn: S. Wright
P.O. Box 73
Lexington, MA 02173

MIT/Lincoln Laboratory — 11
Attn: Dr. D. Hyland
P.O. Box 73
Lexington, MA 02173

MIT/Lincoln Laboratory — 11
Attn: Dr. N. Smith
P.O. Box 73
Lexington, MA 02173

Control Dynamics Co. — 1
Attn: Dr. Sherman Seltzer
Suite 1414 Executive Plaza
555 Sparkman Drive
Huntsville, AL 35805

Lockheed Space Missile Corp. — 5
Attn: A. A. Woods, Jr., D/62-E6
p.O. Box 504
Sunnyvale, California 94088-3504

Lockheed Missiles Space Co. — 1
Attn: Mr. Paul Williamson
3251 Hanover St.
Palo Alto, CA 94304

General Dynamics — 1
Attn: Ray Halstenberg
Convair Division
5001 Keary Villa Rd
San Diego, CA 92123

STI — 1
Attn: Mr. R.C. Stroud
20065 Stevens Creek Blvd.
Cupertiono, CA 95014

NASA Langley Research Ctr — 2
Dr. Earle K. Huckns III
Attn: Dr. Card
Langley Station Bldg 1293B M/s 230
Hampton, VA 23665

NASA Johnson Space Center — 1
Attn: Robert Piland
Ms. EA
Houston, TX 77058

McDonald Douglas Corp 1
Attn: Mr. Read Johnson
Douglas Missile Space Systems Div
5301 Bulsa Ave
Huntington Beach, CA 92607

Integrated Systems Inc. 2
Attn: Dr. N. K. Gupta and M. G. Lyons
151 University Avenue, Suite 400
Palo Alto, California 94301

Boeing Aerospace Company 1
Attn: Mr. Leo Cline
P. O. Box 3999
Seattle, WA 98124
MS 8 W-23

TRW Defense Space Sys Group Inc. 1
Attn: Ralph Iwens
Bldg 82/2054
One Space Park
Redondo Beach, CA 90278

TRW 1
Attn: Mr. Len Pincus
Bldg R-5, Room 2031
Redondo Beach, CA 90278

Department of the navy 1
Attn: Dr. K. T. Alfriend
Naval Research Laboratory
Code 7920
Washington, DC 20375

Airesearch Manuf. Co. of Calif. 1
Attn: Mr. Oscar Buchmann
2525 West 190th St.
Torrance, CA 90509

Analytic Decisions, Inc. 1
Attn: Mr. Gary Glaser
1401 Wilson Blv.
Arlington, VA 22209

Ford Aerospace & Communications Corp. 1
Drs. I. P. Leliakov and P. Barba, MS/G80
3939 Fabian way
Palo Alto, California 94304

Center for Analysis
Attn: Mr. jim Justice
13 Corporate Plaza
Newport Beach, CA 92660 1

W. J. Schafer Associates
Dr. R. Kappesser
Suite 800
1901 Fort Meyer Drive
Arlington, VA 22209 1

General Research Corp
Attn: Mr. Thomas Zakrzewski
7655 Old Springhouse Road
McLean, VA 22101 1

Institute of Defense Analysis
Attn: Dr. Hans Wolfhard
400 Army Navy Drive
Arlington, VA 22202 1

Karman Sciences Corp.
Attn: Dr. Walter E. Ware
1500 Garden of the Gods Road
P.O. Box 7463
Colorado Springs, CO 80933 1

MRJ, Inc.
10400 Eaton Place
Suite 300
Fairfax, VA 22030 1

Photon Research Associates
Attn: mr. Jim Myer
P.O. Box 1318
La Jolla, CA 92038 1

Rockwell International
Attn: Russell Loftman (Space Systems Group)
(Mail Code - SL56)
12214 Lakewood Blvd.
Downey, CA 90241 1

Science Applications, Inc. 1
Attn: Mr. Richard Ryan
3 Preston Court
Bedford, MA 01730

U.S. Army Missile Command 1
Attn: DRSMI-RAS/Mr. Fred Haak
Redstone Arsenal, AL

Naval Electronic Systems Command 1
Attn: Mr. Charles Good
PME_106-4
National Center I
Washington, DC 20360

Lockheed Palo Alto Research Laboratory 2
Attn: Dr. J. N. Aubrun, 0/52-56
3251 Hanover Street
Palo Alto, California 94304-1187

U.S. Army/DARCOM 1
Attn: Mr. Bernie Chasnov
AMC Bldg
5001 Eisenhower Ave
Alexandria, VA 22333

Defense Documentation Center 1
Cameron Station
Alexandria, VA 22314

Honeywell Inc. 2
Attn: Dr. Thomas B. Cunningham
Attn: Dr. Michael F. Barrett
2600 Ridgway Parkway MN 17-2375
Minneapolis, MN 55413

NASA Marshal Space Flight Center 2
Attn. Dr. J. C. Blair, ED01
Henry B. Waites
Marshal Space Flight Center, AL 35812

TRW 1
Attn: Robert Benhabib
Bldg 82/2024
One Space Park
Redondo Beach, CA 90278

MISSION
of
Rome Air Development Center

RADC plans and executes research, development, test and selected acquisition programs in support of Command, Control Communications and Intelligence (C^3I) activities. Technical and engineering support within areas of technical competence is provided to ESD Program Offices (POs) and other ESD elements. The principal technical mission areas are communications, electromagnetic guidance and control, surveillance of ground and aerospace objects, intelligence data collection and handling, information system technology, ionospheric propagation, solid state sciences, microwave physics and electronic reliability, maintainability and compatibility.